MISTRA SWECIA
CLIMATE, IMPACTS & ADAPTATION

SMHI

Reports Meteorology and Climatology

No 113, dec 2008

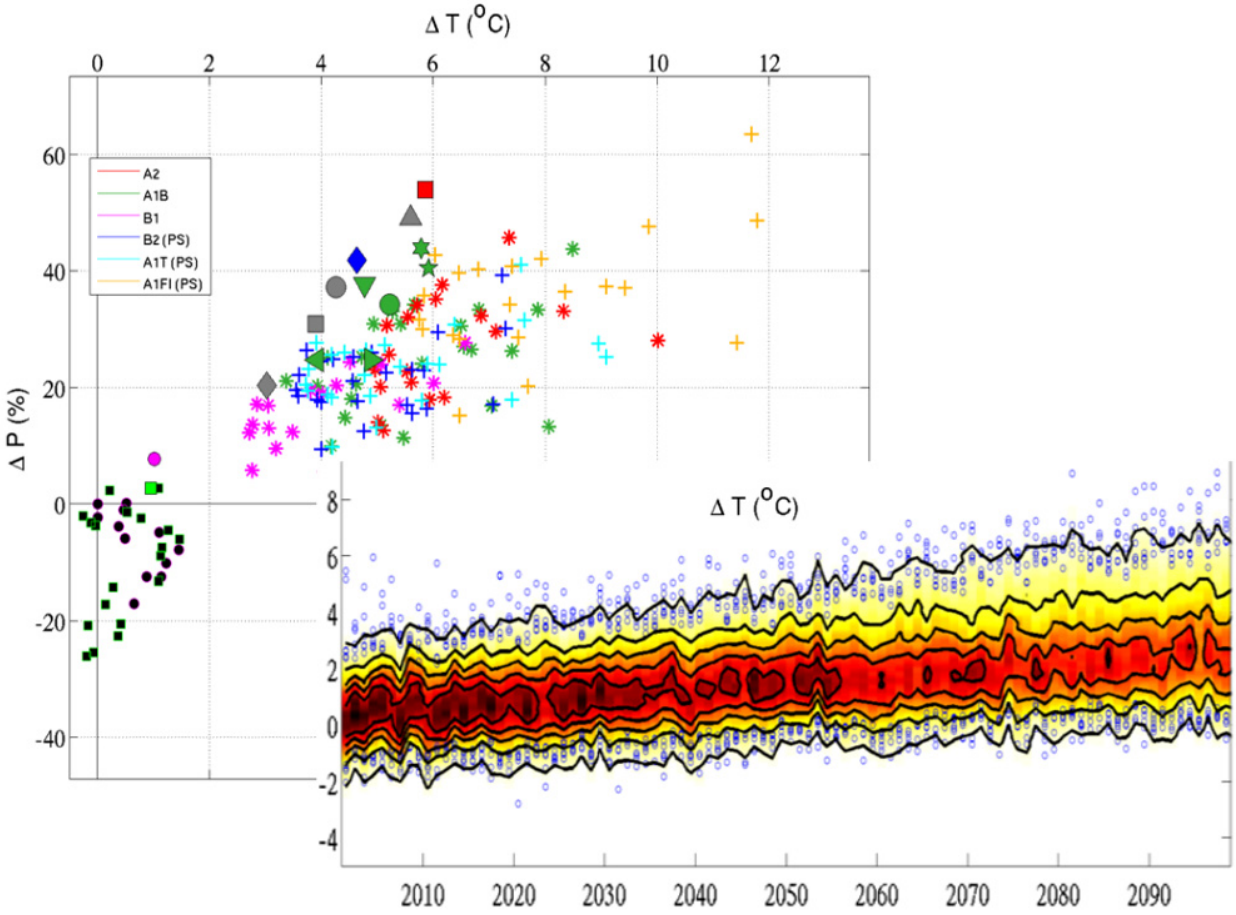

Temperature and precipitation changes in Sweden, a wide range of model-based projections for the 21st century.

Petter Lind and Erik Kjellström

RMK
No 113, dec 2008

Temperature and precipitation changes in Sweden, a wide range of model-based projections for the 21st century.

Petter Lind and Erik Kjellström

Report Summary / Rapportsammanfattning

Issuing Agency/Utgivare

Swedish Meteorological and Hydrological Institute
S-601 76 NORRKÖPING
Sweden

Report number/Publikation

RMK No. 113

Report date/Utgivningsdatum

December 2008

Author (s)/Författare

Petter Lind and Erik Kjellström

Title (and Subtitle/Titel

Temperature and precipitation changes in Sweden; a wide range of model-based projections for the 21st century.

Abstract/Sammandrag

In this report we analyze the climate change signal for Sweden in scenarios for the 21st century in a large number of coupled atmosphere-ocean general circulation models (AOGCMs), used in the fourth assessment report by the Intergovernmental Panel on Climate Change (IPCC). We focus on near-surface temperature and precipitation. The analysis includes six emission scenarios as well as multi-member runs with the AOGCMs. At the Rossby Centre, SMHI, regional climate models have been run under different emission scenarios and driven by a few AOGCMs. The results of those runs have been used as a basis in climate change, impact and adaptation assessments. Here, we evaluate results from these regional climate model runs in relation to the climate change signal of the IPCC AOGCMs.

First, simulated conditions for the recent past (1961-1990) are evaluated. Generally, most AOGCMs tend to have a cold bias for Sweden, especially in winter that can be as large as 10°C. Also, the coarse resolution of the AOGCMs leads to biases in simulated precipitation, both in averages, extremes and often also in the phase of the seasonal cycle. Generally, AOGCMs overestimate precipitation in winter; biases reach 30-40% or even more. In summer, some AOGCMs overestimate precipitation while others underestimate it. Projected responses depend on season and geographical region. Largest signals are seen in winter and in northern Sweden, where the mean simulated temperature increase among the AOGCMs (and across the emissions scenarios B1, A1B and A2) is nearly 6°C by the end of the century, and precipitation increases by around 25%. In southern Sweden, corresponding values are around +4°C and +11%. In summer, the temperature increase is more moderate, which is also the case for precipitation. The regional climate signals are usually within the ranges given by the AOGCM runs, however, the regional models tends to show larger increases in winter, and smaller increases in summertime precipitation.

Key words/sök-, nyckelord

Climate change, transient climate scenario, regional climate modelling, Europe, ENSEMBLES

Supplementary notes/Tillägg

This work has been a part of the Mistra-SWECIA programme and the EU-project ENSEMBLES (GOCE-CT-2003-505539)

Number of pages/Antal sidor

50

Language/Språk

English

ISSN and title/ISSN och title

0347-2116 SMHI Reports Meteorology Climatology

Report available from/Rapporten kan köpas från:

SMHI
S-601 76 NORRKÖPING
Sweden

Contents

1. Introduction

In recent years, the public awareness of the impacts of human activities on climate has increased, in part due to the assessments produced by the UN Intergovernmental Panel of Climate Change, IPCC. The latest assessment, released 2007, concludes that the increase in carbon dioxide in the atmosphere since the mid-1700s, primarily from combustion of fossil fuels and land-use changes, from around 280 to 379 ppmv (2005), has led to levels far above anything experienced over at least the last 650.000 years (IPCC, 2007). Recently this time span has been extended to 800.000 years (Lüthi *et al.*, 2008). Furthermore, the report shows that the global annual average surface temperature between 1906 and 2005 has increased by 0.74°C in the mean. Coupled atmosphere-ocean general circulation models (AOGCMs), have attributed the majority of the temperature increase since the 1950s to human activities. Projections of future changes are produced primarily by simulating the climate in AOGCMs. These tools provide the only physically consistent means for calculating the three-dimensional character of the atmosphere and ocean, and their interaction, and attempt to represent the many physical processes, interactions and feedbacks that determine the climate.

Based on six marker scenarios, consisting of assumptions of, among others, future societal development, IPCC presents studies where continued changes in many climate components are anticipated, and the global mean surface temperature is projected to increase by 1.8 to 4.0°C by the end of the 21st century (2090-2099) relative to the period 1980-1999. These numbers originate from the best estimate of greenhouse gas time series deduced from the six marker scenarios only (Meehl *et al*., 2007). However, the spread between the various climate models, for example AOGCMs, further increases the uncertainty and IPCC assess a likely range that spans a somewhat larger interval; 1.1 to 6.4°C across the given scenarios.

In this report, we discuss three key sources of uncertainty that affect future climate projections from coupled climate models;

- uncertainties associated with the emissions scenarios used to force the models,
- uncertainties related to the model formulations, and
- uncertainties related to natural variability.

In an attempt to represent the emission-related range of uncertainty, IPCC published a number of 40 different scenarios of future rates of anthropogenic emissions, affecting the radiative forcing (Nakićenović *et al.*, 2000). A more complete risk assessment of future climate changes would imply simulations for each of these scenarios, however, due to limited computer resources or perhaps for priority reasons, no such analysis is available today. Out of the assembly of emission scenarios, six marker scenarios were condensed, each representing a distinct direction, i.e. towards globalisation or regionalisation, and/or, towards fossil fuel intensive economies or effective use of resources etc. A thorough analysis of climate change should at least include simulations using all six of these scenarios.

An assessment of the climate responses of the most recent generation of AOGCMs from the climate model intercomparison project CMIP3 reveals a relatively large spread for a given emission scenario both on global and regional scales (Meehl *et al*., 2007; Christensen *et al*., 2007), primarily because of the range in climate sensitivities between the models, the commonly referred metric to determine how the Earth system will respond to a given change in radiative forcing. In large part, the different climate sensitivity in different models is due to the diverse handling and implementation of feedback mechanisms. Internal climate feedback

processes are non-linear and non-additive, either amplifying or dampening the response of the climate system to an external forcing. The full complexity may be addressed by studying only a single or a few feedback processes with simple climate models (SCMs) or Earth system Models of Intermediate Complexity (EMICs), see Randall *et al.* (2007). With a coarser resolution and fewer details computer cost is reduced in such simpler models. Other means to address uncertainties in model formulation include ensemble simulations with one AOGCM with small perturbations in the physical parameterizations in each member (Murphy *et al.*, 2007). The modelling uncertainties (internal feedbacks, discretization on finite grid and parameterisations) are usually manifested through an array of structural choices, for example by differing the grid resolution or using alternative, still physically based, methods to describe sub-grid scale features, such as cloud formation and radiative transfer. Differently to the perturbed physics approach an alternative is to use a multi-model ensemble consisting of several AOGCMs as in CMIP3 or in the ENSEMBLES project (Hewitt and Griggs, 2004). A drawback of the latter approach is that different AOGCMs may share similar parameterizations and thereby biases, or models may lack some processes.

The third major uncertainty is related to internal natural variability of the climate system. There is no reason why an AOGCM should simulate a climate that is in phase with the observed natural variability of the climate. A method to deal with this problem of internal variability is to perform multiple simulations with an AOGCM differing only in initial conditions. As an example the CMIP3 simulations covering the 20th century start in 1860 with different initial conditions. Some of those models are run for several ensemble members giving a range of trajectories for the transient climate change signal in the 20th century and further continuing into the 21st century in the climate change experiments. Such ensembles may thus reflect interannual and interdecadal variability both as observed in the 20th century and as projected for the next decades/century. As the climate change signal increases with time in the future (as the forcing grows) it is expected that the relative role of the internal variability as a source of uncertainty will be smaller (Déqué *et al*., 2007).

Taking all these three major types of uncertainties into consideration a consequence is the need for large ensembles of climate change simulations. Consequently, a prominent aspect of climate modelling which is gaining more attention is the move toward more probability based estimations of future climate signals (Hewitt and Griggs, 2004; Meehl *et al.*, 2007; Christensen *et al*., 2007). As computer resources increases, more models can be run, perhaps with more scenarios, giving means to extending single projections into ensembles and to deduce uncertainties and/or most likely changes of future climate states. Multi-model ensembles should provide an improved basis for these calculations compared to single model ensembles with alternative initial conditions. In view of the unfeasibility to infer the future socio-economic development, technological advances and population changes, a fully probabilistic assessment of future regional climate change involves many scenarios of radiative forcing simulated in as many AOGCMs and with as many separate members (with various initial conditions) as possible. Today, this is not available, and in the near future only to some extent. However, by using a method for scaling a simulated response for a specific scenario, so called pattern-scaling (*e.g.* Ruosteenoja *et al.*, 2003), an increased number of scenarios may be provided. This is done in this report to include the six marker scenarios deduced by the IPCC (see section 2). Still, we remark that the probabilistic scenarios derived in this and other work is conditional in the sense that they are based on a limited set of emission scenarios, AOGCMs and initial conditions. This implies that they do not sample the entire range of uncertainty that is associated with climate change.

Due to the relatively coarse resolution of AOGCMs, of the order of hundred kilometres in the horizontal, the most reasonable scales for meaningfully analysing regional climate signals are continental or sub-continental scales (Randall *et al.*, 2007). At increasingly finer spatial scales the ability decreases, as synoptic and meso-scale features (including storms and fronts) are not resolved properly. In addition, the smooth representation of surface characteristics does not allow the model to capture orographic features (*e.g.* windward rainfall), and land/sea-contrasts in a realistic way. As an example, strong seasonal cycles in precipitation seen on regional and local scales in the Baltic Sea catchment area are not fully captured by AOGCMs (*e.g.* Kjellström and Ruosteenoja, 2007). To complement AOGCMs, other methods that provide climate information at a higher resolution have been developed and improved during the last couple of decades.

The most commonly adopted method to achieve high-resolution information is downscaling large-scale fields. This is done either statistically or dynamically. These approaches have been shown to provide regional and local climate information in good agreement with observations (Christensen *et al.*, 2007; Giorgi *et al.*, 2001, and references therein). The dynamic technique involves the nesting of high resolution models in AOGCMs and has the advantage that meso-scale phenomena, not apparent in the driving fields, may develop without any strong constraints from outside the domain. The large-scale fields are provided by the driving global model or reanalysis at the boundaries. In general, large-scale features of the meteorological fields simulated by the high resolution models do not deviate notably from the driving fields. In the inner part of the domain the regional model has a higher freedom allowing the climate system to evolve relatively independent of the boundary conditions (Kjellström *et al.*, 2005).

The dependence of the downscaling on the large-scale fields provided by the AOGCMs is an important factor; the quality of the downscaled information, and the results, is highly dependent of the quality of the AOGCM data. For instance it can be noted that different large-scale circulation statistics in the global models have a profound effect on the regional climate change signal in for instance near-surface temperature both in the global models themselves (van Ulden and van Oldenburgh, 2006) and in regional climate model integrations (Räisänen *et al*., 2004; Graham *et al.*, 2008).

At the Rossby Centre, at the Swedish Meteorological and Hydrological Institute, different versions of the regional climate model RCA have been used in downscaling-experiments. Recently, a report was released by the Swedish government, containing results from an extensive investigation of possible climate change and impacts in Sweden (SOU, 2007). The projections of future climate change in Sweden were provided by RCA, run under, and driven by, a number of scenarios and AOGCMs (Persson *et al.,* 2007). The patterns of temperature and precipitation change in the 21st century in Sweden, as simulated in RCA, have been discussed in several other studies (*e.g.* Räisänen *et al.*, 2004; and Kjellström *et al.*, 2005). There are both clear regional differences (north versus south) and seasonal patterns. Generally, results show that the surface temperature increases in the whole of Sweden and in all seasons, however, the signal is greater in winter. Furthermore, the response is clearer in the northern region. This is due to the concurrent simulated change in the snow climate, for example a shorter snow season affecting the energy budget at the surface, which is more prominent in the colder northern Sweden. The precipitation change depicts a considerable increase in winter (a warmer climate with more moisture in the cold season) and a smaller increase, or a decrease in the south, during summer.

In this report, these regional climate change scenarios for Sweden are put into a wider perspective by comparing them to results from several AOGCMs used in the IPCC assessment. The regional climate model runs include additional runs with boundary conditions from more than one AOGCM. Two primary climate variables are investigated, both for the control period and the 21st century; surface temperature and precipitation.

2. Data

Here we describe the different data sets used in the report. These are; i) the CMIP3 data consisting of data from more than 20 AOGCMs forced by different emissions scenarios, ii) the regional climate change scenarios from the Rossby Centre model RCA, iii) evaluation data and iv) a set of scaling factors from a simple climate model used for expanding the number of scenarios with the pattern-scaling technique described in chapter 3. All data used in this report are either on a monthly or a seasonal mean basis. In most of the subsequent analysis a subdivision is performed into a southern and northern region, determined approximately by the flow of river Dalälven (Fig. 2.1), as to further investigate the regional differences in climate change in Sweden. The larger islands of Gotland and Öland in the Baltic Sea are excluded in the analysis.

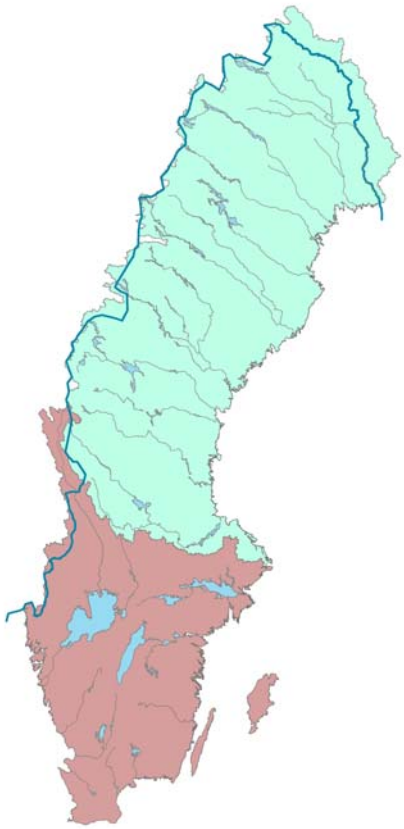

Figure 2.1. *The analyzed regions; the northern part of Sweden (blue-green) is separated from the southern part (red) approximately by the flow of river Dalälven, constituting a natural hydrological division line in terms of the discharge into the Baltic Sea. The islands of Gotland and Öland in the Baltic Sea (red colored) are not included in the analysis.*

2.1 AOGCMs and emissions scenarios

The scenarios used to force the AOGCMs in the simulations are outlined according to certain assumptions concerning, among others, the energy use, demand and sources in the future, societal and technological development, and changes in world-population (Nakićenović *et al.*, 2000). A total of 40 different scenarios have been published in an attempt to produce a comprehensive expression of alternative future emission rates. Even though none of these scenarios were assigned probabilities, six marker scenarios were defined considered to represent the range of high to low emissions in the 21st century, in descending order; A1FI, A2, A1B, A1T, B2 and B1. Due to restricted computer resources, three out of the six scenarios, A2, A1B and B1, were selected to produce the AOGCM multi-model projections used in the AR4 assessment (Meehl *et al.*, 2007).

The AOGCM simulations are run from mid 19th century to the year 2100. For the 19th and 20th century simulations, the time evolution of concentrations of long-lived greenhouse gases and aerosols are constrained in large part by observations, and consequently the historical change of the radiative forcing is quite similar in all models. For the scenarios, the concentrations of GHGs are calculated by running the emission time series off-line in various biogeochemical models. Aerosol precursors, in essence the emission of sulphur dioxide, are either simulated explicitly within the models atmospheric chemistry processes, or extracted from estimates in runs with simple, specialised chemical models (Meehl *et al.*, 2007). Radiation schemes and different parameterisation components finally convert the concentrations of greenhouse gases and aerosols to radiative forcing for the respective scenario.

Uncertainties associated with the defined scenarios and thus the radiative forcing can not be analysed feasibly, l*et al*one be quantified, as assumptions of factors that determine the emissions of GHGs and aerosols are highly uncertain. Increasing the number of scenarios is therefore desirable in order to better sample the full uncertainty range and producing more data to be used in probabilistic studies. Simulations from 24 different AOGCMs are used together with the six marker scenarios mentioned above (Table 2.1). Not all six scenarios have been simulated in the models, however, in this study, the full set of emission scenarios are obtained through pattern-scaling (see section 3.2). The AOGCM data was available from the World Climate Research Program's (WCRP's) Coupled Model Intercomparison Project phase 3 (CMIP3) multi-model dataset (hereafter referred to as the CMIP3 data). The models are all fully three-dimensional AOGCMs, documented in peer-review literature and have participated in the CMIP3 project (*e.g.* Meehl *et al.*, 2007).

Table 2.1. *AOGCMs in this report. TXX denotes the truncation number, where XX is the maximum number of waves resolved in the horizontal along a latitude circle. In Levels, A/O signifies the number of vertical levels in the atmosphere/ocean. In the last column, the simulated scenarios are presented, where the number of simulations for each scenario is given in parenthesis. References for the models can be found in Meehl et al., 2007.*

Model	Country	Atm. res.	Ocean res.	Levels	Scenarios
BCCR-BCM2.0	Norway	T63	0.5-1.5° × 1.5°	A31, O35	A1B(1), A2(1), B1(1)
CCSM3	USA	T85	0.3-1° × 1°	A26, O40	A1B(7), A2(5), B1(9)
CGCM3.1	USA	T47	1.9° × 1.9°	A31, O29	A1B(5), A2(5), B1(5)
CGCM3.1 (hires)	USA	T63	0.9° × 1.4°	A31, O29	A1B(1), B1(1)
CNRM-CM3	France	T63	0.5-2° × 2°	A45, O31	A1B(1), A2(1), B1(1)
CSIRO-MK3.0	Australia	T63	0.8° × 1.9°	A18, O31	A1B(1), A2(1), B1(1)
CSIRO-MK3.5	Australia	T63	0.8° × 1.9°	A18, O31	A1B(1), A2(1), B1(1)
ECHAM5 / MPI-OM	Germany	T63	1.5° × 1.5°	A31, O40	A1B(3), A2(3), B1(3)
ECHO-G	Ger./Korea	T30	0.5-2.8° × 2.8°	A19, O20	A1B(3), A2(3), B1(3)
FGOALS-g1.0	China	T42	1° × 1°	A26, O16	A1B(3), B1(3)
GFDL-CM2.0	USA	2.0° × 2.5°	0.3-1° × 1°	A24	A1B(1), A2(1), B1(1)
GFDL-CM2.1	USA	2.0° × 2.5°	0.3-1° × 1°	A24	A1B(1), A2(1)
GISS-AOM	USA	3° × 4°	3° × 4°	A12, O16	A1B(2), B1(2)
GISS-EH	USA	4° × 5°	2° × 2°	A20, O16	A1B(3)
GISS-ER	USA	4° × 5°	4° × 5°	A20, O13	A1B(2), A2(1), B1(1)
INM-CM3.0	Russia	4° × 5°	2° × 2.5°	A21, O33	A1B(1), A2(1), B1(1)
IPSL-CM4	France	2.5° × 3.75°	2° × 2°	A19, O31	A1B(1), A2(1), B1(1)
MIROC3.2	Japan	T42	0.5-1.4° × 1.4°	A20, O43	A1B(3), A2(3), B1(3)
MIROC3.2 (hires)	Japan	T106	0.2° × 0.3°	A56, O47	A1B(1), A2(1), B1(1)
MRI-CGCM2.3.2	Japan	T42	0.5-2.0° × 2.5°	A30, O23	A1B(5), A2(5), B1(5)
NCAR-PCM	USA	T42	0.5-0.7° × 1.1°	A26, O40	A1B(4), A2(4)
HadCM3	UK	2.5° × 3.75°	1.25° × 1.25°	A19, O20	A1B(1), A2(1), B1(1)
HadGEM1	UK	1.3° × 1.9°	0.3-1° × 1°	A38, O40	A1B(1), A2(1)
INGV-ECHAM4	Italy				A1B(1), A2(1)

Since the third assessment report (IPCC, 2001), models have improved in several aspects, primarily through increased resolution, both horizontally and vertically, better parameterisation of clouds and inclusion of more processes, including more elaborate sea ice dynamics and thermodynamics (Randall *et al*., 2007). Furthermore, representation of aerosol distribution and atmospheric chemistry has been improved. Most of the models in the previous report used flux adjustments of surface heat, water and momentum to avoid climate drift and thus destabilisation of simulations. Due to the modifications and improvements mentioned the many of the 24 AOGCMs operates without these adjustments.

The coarse scale in the AOGCMs complicates a straightforward comparison with RCM data. One example is the poor resolution of the Scandinavian mountain chain that is almost absent in the models with coarse resolution. In the most high-resolved AOGCM, MIROC3.2(hires), and the RCMs there is a mountain chain that has a profound impact on the precipitation distribution in this area. Another example is the land-sea mask. In some AOGCMs the Baltic Sea is poorly resolved, or in some cases, completely absent. For that reason, the land-sea masks of all the AOGCMs are looked at with the intention of examining how reasonably the models represents the northern and southern parts of Sweden. All the land-sea masks are presented here to visualize the differences between high- and low-resolution models in this area (Fig. 2.2).

The Japanese high-resolution model, MIROC 3.2(hires), resolves the European domain quite well with a reasonable land-sea distribution including some large inland lakes, most evidently Lake Ladoga and Lake Onega in Russia and Lake Vänern in Sweden. The contrast is rather dramatic when comparing with ECHO-G that has a lower resolution (T30, around 400 km). Here, the land/sea-mask over Europe is very coarse. Large discrepancies are obvious near inflows to the Mediterranean Sea, the Black Sea and the Baltic Sea. For the latter area neither Denmark nor the southern-most part of Sweden exists as land-areas. In summary, many models have relatively poorly resolved land and sea-contrasts in the Scandinavian region. This is particularly the case for ECHO-G, INM-CM3 (similar to ECHO-G) and FGOALS (in which the Baltic Sea is completely absent). Further, the discrepancies are most often larger in southern Scandinavia, a fact that may influence the results for this region.

The consequences of the different land-sea masks in the different models are ambiguous. In the control period (1961-1990), no clear deviations in the precipitation climate between observations (ERA40 and CRU) and the ECHO-G model occurs that could be explained by the low resolution (Section 4.1). In case of surface temperature, ECHO-G shows a pattern that indicates a weaker seasonal cycle compared to ERA40 both in north and in south but more prominently in the south. To some extent, this could indicate a more maritime influenced climate in this region in ECHO-G compared to ERA40 in line with the coarse land-sea mask. Nonetheless, the deviation in this AOGCM is not, by far, the one that deviates the most from the other AOGCMs, and, thus, the low resolution by itself does not support any exclusion of this model in the analysis. Northern Europe winter temperatures in FGOALS are abnormally cold (see Section 4.1), thus, climate information from FGOALS should be examined with care. In any case, no models are excluded based only on their resolution of land and sea in the analysed domain, but these should be borne in mind.

In order to facilitate evaluation of the regional signal in relation to regional climate models the AOGCMs have been interpolated to a common grid, the RCA3 grid (see section 2.2). Further information on the structure, performance, results and references to current literature of the

AOGCMs can be found in chapter 8, 10 and 11 in the latest IPCC report (Randall *et al.*, 2007; Meehl *et al.*, 2007; Christensen *et al.*, 2007).

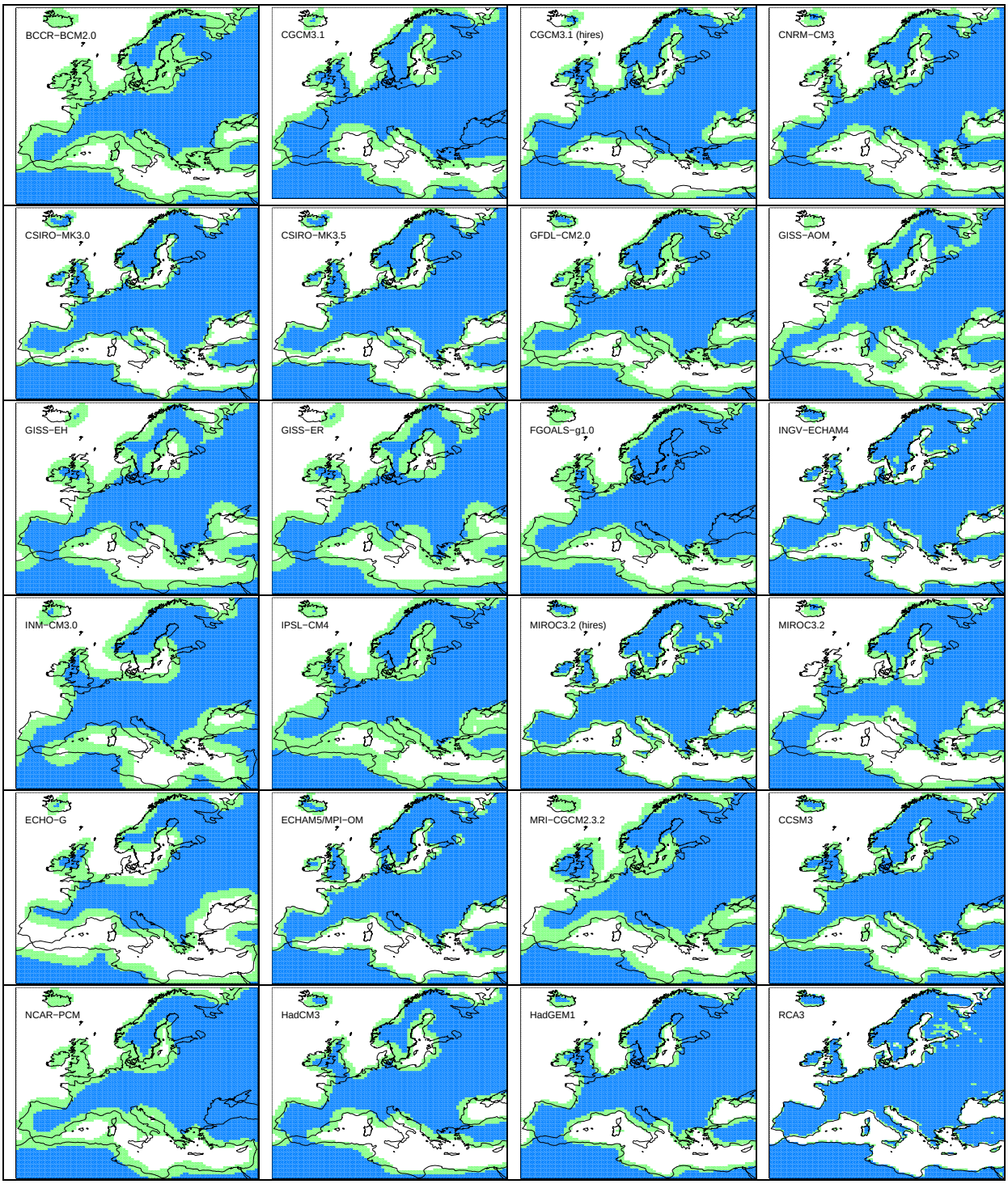

Figure 2.2. *Land-sea masks on the RCA3 grid. The original land-sea masks in the AOGCMs have been interpolated to the RCA3 grid. Land fractions above 50% (75%) are denoted by green (blue).*

2.2 Regional climate models

Two versions of the Rossby Centre regional climate model are considered in this analysis; RCA3 (Kjellström *et al.*, 2005) and RCAO (Döscher *et al.*, 2002). The former is the latest version of the atmospheric model system and the latter is a coupled atmospheric-ocean model. RCA3 has been undergoing some important changes compared to its predecessor RCA2 (Jones *et al.*, 2004). The main part of the dynamic structure and physical representation is retained but changes in parameterisations of clouds, radiation and turbulence have been implemented. The RCA model is based on the operational high resolution limited area model HIRLAM (Källén, 1996), with necessary structural reworking or replacements to allow the model to properly run in climate mode. It also includes a land surface model (Samuelsson *et al.*, 2006) and a lake model, PROBE (Ljungemyr *et al.*, 1996), describing the interaction with the numerous inland lakes in the area.

The RCA3 model has been run on a rotated latitude-longitude grid with a horizontal resolution of 0.44°, corresponding to approximately 49 km, and a hybrid vertical coordinate system; terrain-following in the lower troposphere and pressure-following in the upper troposphere, consisting of 24 levels up to 10 hPa. The simulation is performed over a model domain covering Europe represented by 102x111 grid boxes used also in the ENSEMBLES project (Hewitt and Griggs, 2004), the outermost eight on each side used as a boundary relaxation zone. The integration time step is set to 30 min (Kjellström *et al.*, 2005).

The coupled regional climate model RCAO consists, in addition to the atmospheric component RCA2 (Jones *et al.*, 2004), of a three-dimensional ocean model, RCO (Meier *et al.*, 1999; Meier *et al.*, 2003). The ocean model component is run over an area covering the Baltic Sea and Kattegat, with a horizontal resolution of 6 nautical miles (nm) corresponding to about 11 km, and 41 vertical layers. The atmospheric component was run on a rotated latitude-longitude grid with the same resolution as RCA3, however on a slightly shifted grid, used in the PRUDENCE project (Christensen and Christensen, 2007) (106 x 102 grid boxes; the eight outermost points constitutes a boundary relaxation zone). The RCAO data have been interpolated to the RCA3 grid described above to enable a direct comparison with RCA3 and the AOGCMs.

Table 2.2. *The 17 regional climate model simulations that are put into a wider perspective in this report.*

RCM	Forcing AOGCM	Time period	Emission scenario	Reference
RCA3	ECHAM4	1961-2100	A2, B2	Kjellström *et al.*, (2005)
RCA3	ECHAM5	1950-2100	A1B (3 runs)	Kjellström *et al.*, (2005)
RCA3	ECHAM5	1950-2100	B1	-
RCA3	CNRM	1950-2100	A1B	-
RCA3	HadCM3 (ref)	1961-2099	A1B	-
RCA3	HadCM3 (low)	1961-2099	A1B	-
RCA3	HadCM3 (high)	1961-2099	A1B	-
RCA3	CCSM3	1961-2100	A2, A1B, B1	-
RCAO	ECHAM4	1961-1990, 2071-2100	A2, B2	Räisänen *et al.*, (2003)
RCAO	HadAM3H	1961-1990, 2071-2100	A2, B2	Räisänen *et al.*, (2003)

Several runs have been performed, with both RCA3 and RCAO, where boundary conditions have been provided by different AOGCMs. The three runs with the RCA3 model driven by ECHAM5 model on the boundaries differ from each other only in that the three separate ECHAM5 simulations differs in initial conditions. The three HadCM3 simulations termed (ref, low and high) are from the Hadley Centre perturbed physics ensemble (Collins *et al*., 2006). The difference between them is that the parameter settings in HadCM3 differs somewhat leading to weaker (low) or stronger (high) response to the changing radiative forcing compared to the reference (ref) version. In the case of RCAO, no transient runs were available and, thus, only time slice experiments can be used in this report (Table 2.2). It should be noted that out of the 17 experiments listed in Table 2.2 it is only the five ones forced by ECHAM5 and CNRM that have boundary data that are identical to those used for the corresponding AOGCMs in the IPCC AR4 and analysed in this report. For all other downscaling experiments boundary conditions are taken from simulations with AOGCMs that have not been part of AR4.

2.3 Evaluation data

Results from the AOGCMs are first compared to reference data sets for the end of the 20th century in order to assess how realistic they are. The reference data sets used for this evaluation consist of observational data sets, quasi-observations like reanalysis data and other model generated data.

A nearly 150 year long time series of surface temperature and precipitation for Sweden, hereafter called SMHI data (Alexandersson, 2002) is used for model evaluation and illustration of decadal variability. The record consists of 29 temperature stations and 87 precipitation stations distributed across the land area, although the density varies quite significantly between the southern and the northern parts of Sweden and between coastal and mountainous areas. The observational record starts in 1860 and extends to the year 2005. During this time, methods of measurements and technological innovations have progressed leading to artificial trends and discontinuities. In addition to a more systematic selection of stations (in order to avoid erroneous and low quality measurements), these artefacts are corrected for in the record through the application of a Standard Normal Homogeneity Test (*e.g.* Alexandersson and Moberg, 1997). It utilises the correlation and covariation of meteorological variables between closely located stations and regions. Through the homogeneity test, deviations from these covariations can be detected and corrected for. Sudden changes or trends may occur, among other things, during relocation of measurement sites, both locally and regionally, and instrument modifications. The latter is more prominent for precipitation. Earlier, in the beginning of the record, precipitation was measured with collectors that were not equipped with wind shields, thus underestimation was a serious problem especially during winter. To add further observational information of the natural variability, the gridded CRU TS 2.1 data set (Mitchell and Jones, 2005) for surface temperature and precipitation have been included. That record covers the period 1901-2002 and has a horizontal resolution of 0.5°×0.5°.

Spatial averages for the observational data have been calculated for two regions, separating northern and southern Sweden (Fig 2.1). The corrected temperature and precipitation values have been condensed into partly overlapping 30-year means during the period 1860-2005 so as to increase the number of tri-decadal means that will be used in the comparison with model simulated time-slice means. This led to a total number of twenty averages (1862-1891, 1868-1897, …, 1976-2005), for yearly and seasonal time periods for the SMHI data and 13

averages (1901-1930, 1907-1936, …, 1973-2002) for the CRU data. The 30-year averages were calculated relative to the 1961-1990 base line value and thus constitute anomalies in °C (temperature) and percent (precipitation). Both these two datasets are used to illustrate the decadal variability during the 20th century. It should be noted that this is not just governed by "pure" natural variability as the external forcing due to human activities has been changing over this period. However, we note that the variability in this area is large already in the early parts of the 20th century reflecting the fact that the natural variability is large in this area.

Reanalysis data consists of output from a numerical weather prediction (NWP) model. The NWP model makes use of observational information through the process of data assimilation. In this way the end product is a physically consistent data set that closely follows the evolution of the atmosphere. In this report we use data from the European Centre for Medium Range Weather Forecasts (ECMWF) reanalysis product ERA40 (Uppala *et al*., 2005). The ERA40 data set covers the time period 1958-2001. As the horizontal resolution of the ERA40 data is relatively coarse (grid spacing of about 110 km) we also use data from a downscaling experiment in which the regional climate model RCA3 (see section 2.2 above) was forced at its lateral boundaries by ERA40 data. The resulting RCA3 data set has a horizontal resolution of 50 km.

2.4 Scaling factors for pattern-scaling

The pattern-scaling technique described below in section 3.2 constitutes a technique to estimate the response to climate change in scenarios that have not been explicitly simulated by fully coupled AOGCMs. A requirement is that scaling-factors relating the change in global mean temperature in such AOGCM scenarios are related to other scenarios that have been calculated. In this work we use scaling factors calculated with the Model for the Assessment of Greenhouse-gas Induced Climate Change (MAGICC) energy balance climate model (Wigley, 1994). We note that the AOGCMs used in the IPCC Fourth Assessment Report have different climate sensitivities. Due to these differences, the MAGICC simulations should emulate responses in each of the AOGCMs. However, no such data were available in this study. Instead, the average of MAGICC-emulated global mean temperature series for four AOGCMs used in the Third Assessment Report (Cubasch *et al.*, 2001) is used here. These models are; CSIRO Mk2, ECHAM4, HadCM3 and NCAR PCM. The average climate sensitivity, measured as the equilibrium response in global mean temperature for a doubling of atmospheric CO_2 concentrations, for these four models is 2.8. This number could be compared to 3.3 as an average for 19 of the AR4-models listed in Table 2.1 (cf. Table 8.2 in Randall *et al.,* 2007). As both these average climate sensitivities and also the spread between the models are fairly similar we assume that the difference in source of information about the climate sensitivity does not have a major impact on the presented results. The global annual mean temperature is calculated for each of the six marker scenarios and for the time period 1960-2099. In the pattern-scaling method, only the ratios between temperatures in different scenarios are important (see next section), and this allow the average of four AOGCMs to be used even though the absolute changes may differ significantly between these.

3. Method and analysis

3.1 Evaluating model performance in the recent past

In assessing the climate change signal in an AOGCM, or any other type of climate model for that matter, one needs to evaluate the performance and skill of the models. An often used method is to investigate the models ability to simulate the recent past climate by comparing model results with observations, whereby biases and deficiencies in simulated variables may be detected at a variety of spatio-temporal scales. Important here, is that all models experience some degree of unpredictable internal variability that may or may not be "in phase" with the observed natural variability (this is the third of the major uncertainties discussed in the introduction). This could misleadingly be interpreted as biases in the simulated climate due to deficiencies in the model itself. Instead, in assessing the models skills, one needs to take into the account the differences due to the internal variability. In other words, differences should be considered insignificant if they are within this variability, and also within the observation error limits.

As the climate in northern Europe is highly determined by the large-scale circulation we look at the AOGCMs ability to simulate this circulation by investigating patterns of mean sea level pressure. The surface pressure field in the region has some specific features like the Siberian winter high/summer low and the semi-permanent low-pressure area south of Iceland and the corresponding high-pressure region off the coast of Portugal. This dipole pressure pattern over the North Atlantic governs the north-south surface pressure gradient, described by the NAO-index, controlling the large scale circulation over Europe, especially in winter. In autumn and winter, synoptic-scale low-pressure systems formed over the North Atlantic frequently enter Scandinavia from the west. Almost all the precipitation that falls in the winter season originates from these systems, and, therefore, capturing these in climate models is important. In summer, on the other hand, the high-pressure pattern moves north-ward leading to more anti-cyclonic conditions over Scandinavia. The generation of precipitation is therefore more locally generated through convective processes.

The RCMs closely follow the AOGCMs in their representation of the large-scale circulation. As the recent past climate in RCAO and RCA3 has been described elsewhere (*e.g.* Räisänen *et al*., 2003, Kjellström *et al.*, 2005) we focus on the evaluation of AOGCMs in this report.

3.2 Pattern-Scaling

The technique of pattern-scaling provides a possibility to increase the number of scenarios and time periods from a restricted set of simulations with an AOGCM or RCM. In principle, the technique involves obtaining a spatial pattern of a climate change signal from an existing AOGCM (or RCM) simulation, and scaling the magnitude of the change using global annual mean surface temperature obtained with a simple climate model run in the scenario you want to obtain, i.e. the target scenario. This is an intriguing method, which has been proven to give reasonably good results for the two main climate variables, temperature and precipitation, on annual as well as seasonal time scales (Mitchell, 2003). However, these methods are only valid under certain assumptions. The two primary assumptions are;

1. The global climate change signal in the AOGCM is accurately represented in the simple climate model, which is used to provide the magnitude of the response. This should hold even in the non-linear responses as well.
2. The independence of the geographical pattern of the climate change to the forcing. The response to the radiative forcing in an AOGCM, of a wide range of climate variables, at regional, local and seasonal scales is a strictly linear function of the amount of global warming.

The second assumption is the most critical and at the same time the most difficult to validate, as local responses of a range of meteorological variables, including temperature and precipitation, may not be essentially linear functions of global mean temperature. Several factors may influence the pattern-scaled responses; one of these is the impact of natural variability (Kjellström *et al.*, 2005). Furthermore, different scenarios may end up at the same amount of global warming even if the pathway to this change can be significantly different. Such differences in pathways, introduced by differences in for instance the rate of greenhouse-gas changes and duration, i.e. length of time, of the forcing, all can introduce errors in the scaling procedure.

In the model simulations the natural variability is an integrated part of the climate evolution, and thus is transferred into the scaled signals. This random noise is greater on the regional or local scale, especially for precipitation and on shorter time scales such as decadal means. Therefore, long time series of simulated and observed data is required to be able to clearly define the noise from this variability and thus to allow identification of errors in the scaling procedure. The separation of noise into natural variation and scaling error is not explicitly done here; instead it is assumed that most of the internal variability is removed through the use of an ensemble method (see next section), and deviations should be interpreted as errors in the scaling.

For each target scenario (x), the anomaly in a variable V (ΔV) relative a long-term mean (usually the 1961-1990 time period), in a grid point (i), season (j) and year or period (y) is given by

$$\Delta V_{xijy} = S_{xy} \cdot V'_{zij} \tag{1}$$

where (z) is the same or another scenario than the target scenario. S represents the scaling factor, i.e. the ratio of the global temperature anomaly between the target scenario and the existing scenario, for the specific time period. V' is the response pattern relating the local change to the global change. The scaling factors are derived from runs with a simple climate model (SCM), see Chapter 2.4.

3.2.1 Super-ensemble pattern-scaling

There are a number of different methods to calculate the response pattern (V' in Eq.1). Traditionally, a simple time slice method is utilised, in which the spatial response for a specific time period is deduced employing only one single signal from a GCM as in Eq. 1. However, in order to reduce the influence of the noise in the model simulations several runs (with the same GCM), i.e. an ensemble mean instead of individual responses may be used. Ruosteenoja *et al.* (2007) apply this method in a similar study, and they go even further to increase the ensemble size by including GCM responses from several SRES scenarios in a

least-square regression line to calculate the regional change pattern. So, for temperature, the scaled response for a specific GCM, scenario and time period, is given by

$$\Delta T_{xijy,s} = a_T \cdot < \Delta T_{xy} >; \tag{2}$$

$$a_T = \frac{\sum_{k=1}^{n} < \Delta T_k > \cdot \Delta T_{kijy,g}}{\sum_{k=1}^{n} < \Delta T_k >^2}, \tag{3}$$

where subscript *s* and *g* refers to scaled and simulated responses respectively. The < > symbolises the MAGICC global mean temperature anomalies with reference to the 1961-1990 baseline period, and *k* is the various runs and scenarios. The same procedure is applied for precipitation, now switching the simulated regional temperature ($\Delta T_{kijy,g}$) to simulated precipitation ($\Delta P_{kijy,g}$) but retaining the global mean temperature anomalies from MAGICC in Eq. 3. Although more of the noise due to internal natural variability may be filtered out the greater the ensemble, at the same time the risk of missing non-linear effects when including emission scenarios with significantly less emissions than the target scenario, i.e. in extrapolation, increases. Ruosteenoja *et al.* (2003; 2007) and Mitchell (2003) discuss the problems related to the extrapolation versus interpolation procedure. They agree that, generally, when using only one single scenario it is better to scale from a scenario as 'close' as possible to the target scenario and also from a stronger to a weaker forcing scenario, for example scaling from an A2 to a B1 scenario.

The super-ensemble method is applied here as data from several members and scenarios is available in most AOGCMs (Table 2.1), allowing a larger ensemble to be produced. A simple approach to check if the resulting responses from the pattern-scaling procedure are reliable, one may compare the simulated climate change signal for a specific scenario in a specific AOGCM to the pattern-scaled signal for the same scenario and model. We do this for the A2, A1B and B1 scenarios, as these were simulated.

Generally, most pattern-scaled data are in good agreement with the simulated data for all seasons. The best agreement is achieved for temperature and for distant time periods. The agreement is somewhat worse for precipitation and for near future. Overall, the temperatures do not deviate more than around a half degree Celsius, and precipitation estimates are within 15 % from each other. This lends confidence to the pattern-scaling method as a provider of additional scenarios to the analysis. Some of the results of these comparisons are presented here as to give an indication of the accuracy of the scaling method. Figs 3.1 and 3.2 give a sample of analyses including pattern-scaled B1 and A2, for different time periods and a few models, namely CGCM 3.1 (T47), INM-CM3 and ECHAM5.

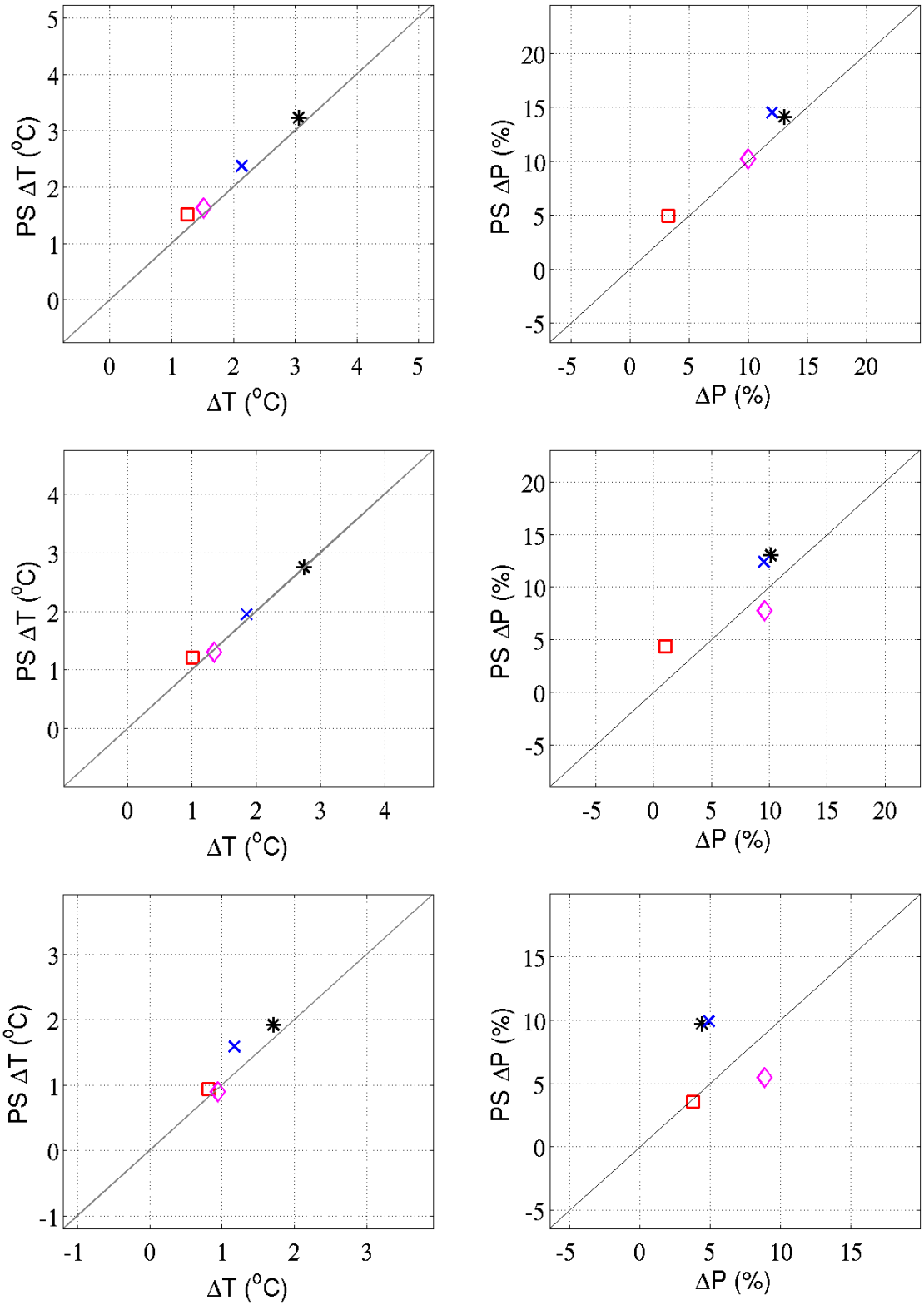

Figure 3.1. *Pattern-scaled (PS) data compared with the corresponding simulated data. Seasonal mean changes in temperature (left) and precipitation (right) compared to 1961-1990 are shown for; 2011-2040 (bottom), 2041-2070 (middle) and 2071-2100 (top). Results are presented for the CGCM 3.1 (T47) model, in northern Sweden, under the B1 emission scenario. The black, blue, red and magenta colored markers represents winter (DJF), spring (MAM), summer (JJA) and autumn (SON) respectively.*

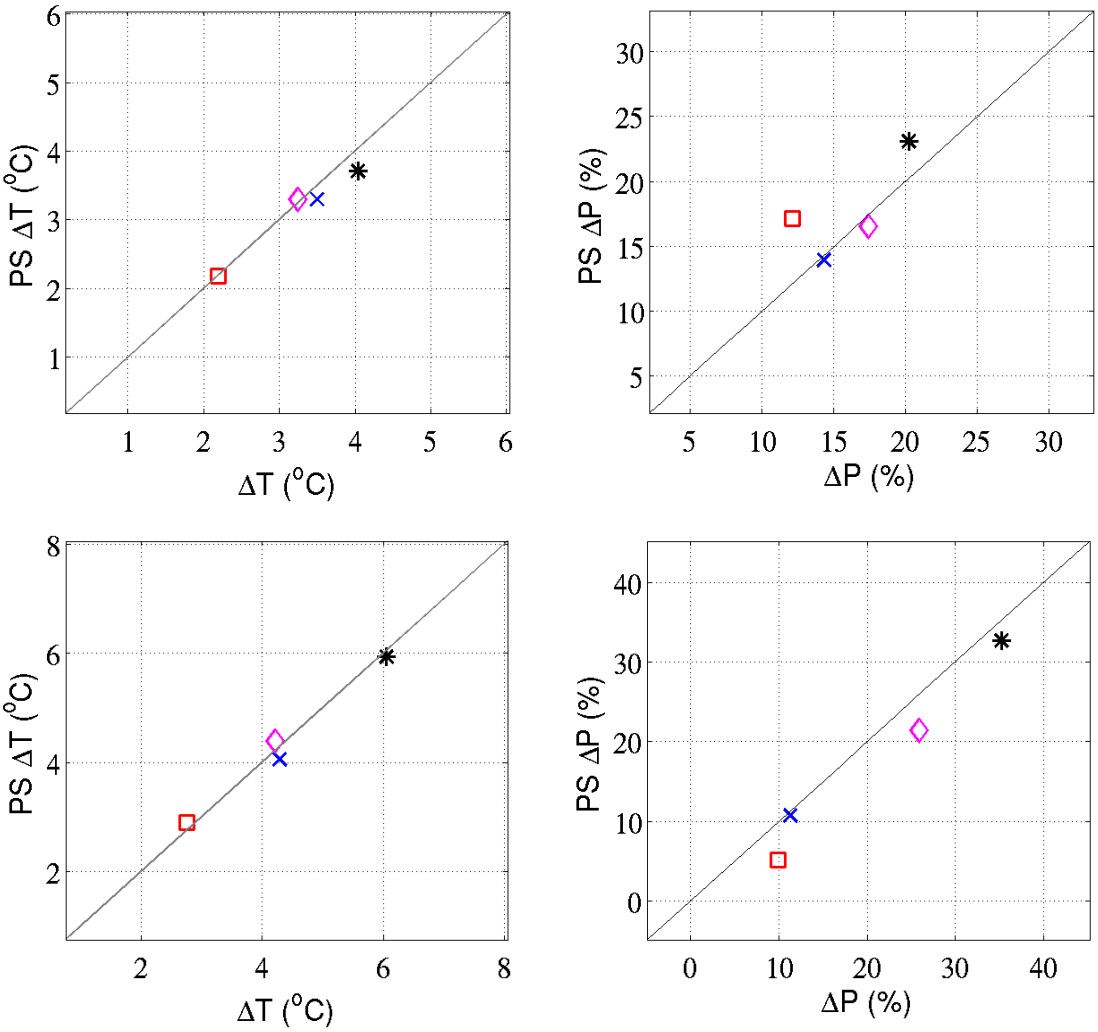

Figure 3.2. *Pattern-scaled (PS) data compared with the corresponding simulated data. Results for the years 2071-2100 in the A2 scenario for seasonal mean temperature (left) and precipitation (right) changes compared with 1961-1990 are shown. The upper panels show results with INM-CM3 for southern Sweden and the lower panels show results for ECHAM 5 for northern Sweden. The black, blue, red and magenta colored markers represents winter (DJF), spring (MAM), summer (JJA) and autumn (SON) respectively.*

3.3 Scatter-plots

The climate change signals for each of the four seasons are calculated by subtracting the baseline (1961-1990) tri-decadal mean from the mean values of the projections of temperature and precipitation for three equally long time slices; 2011-2040, 2041-2070 and 2071-2100. In the case of precipitation, the difference is normalised with the mean from the baseline period, giving the change in percent. It is worth noting here that when comparing relative changes in precipitation between different seasons, one should be aware of the absolute values of precipitation in the respective season. For example, winter values are lower than in summer, and future relative changes might then artificially appear to be amplified in winter compared to summer. The information is presented for the two regions in Sweden in scatter diagrams. In these, the change in surface temperature is given on the ordinate and relative precipitation changes are represented on the abscissa. For every scenario the simulated climate response in the AOGCMs and in the RCMs is depicted by a marker in the scatter plot, indicating the joint

temperature/precipitation change. Three different sets of scatter plots are produced; single-scenario, multiple-scenario and multi-member diagrams. The latter illustrates the individual members of a single GCM in order to illustrate the sensitivity related to initial conditions. However, only the control climate is investigated in this aspect, in order to estimate the relative importance of internal variability (see Section 4.1.4).

3.4 Principal Component Analysis (PCA)

A method to increase the ensemble size through production of additional climate scenarios out of a smaller set of simulations is to decompose the original ensemble into independent components describing the statistical properties of the ensemble. These components may then be randomly resampled and recombined a large number of times in a Monte Carlo approach and consequently increasing the ensemble size. We achieve the decomposition through the use of a principal component analysis (PCA) following Dettinger (2006).

The main advantageous property of the PCA-method is the orthogonality that characterises the decomposed components from the original ensemble. Through this, the resampling method allows an almost unlimited number of "new" realisations (scenarios) to be produced, enough to construct smooth probability-density functions (pdfs), while, importantly, retaining the essential first and second order statistics including the time evolving mean and standard deviation as well as correlations (Dettinger, 2006).

A more mathematical presentation of the method is available in Dettinger (2006) and is, therefore, left out here. Still, a short description of the procedure is suitable for introducing the reader to the structure of the method and handling of the data. Here, the available data originates from several AOGCMs, run in three different emission scenarios (A2, A1B and B1) and in some cases for more than one member. We use anomalies compared to the 1961-1990 mean for each season or year for the hundred-years time period 2000-2099. Accordingly, the matrix of simulated data consists of a number of columns with different runs (AOGCMs, scenarios and members) and rows representing each time step (year or season) in the integration. As a first move in the procedure, the ensemble mean in each time step is calculated and subtracted from the corresponding row-vector, to establish a centred, i.e. zero-mean, ensemble. Similarly, the standard deviation for every time step is calculated and then used to normalise the centred scenarios. By performing these two measures, the first two statistical moments have been removed, to be included later on in the newly produced scenarios, and, thus, the variability and time evolution mean are retained in the larger resulting ensemble.

Furthermore, a correlation matrix is generated, through computation of cross correlation between the various time steps for every member with expectation values taken across the ensemble. The resulting matrix is then run through a PCA-analysis, whereby the members are decomposed into definitely independent normalised empirical-orthogonal functions (EOFs), and a corresponding coefficient matrix consisting of values that give the strength, or weight, of a specific component. If, for example, a third of the members show trends in surface temperature towards cooler climate, one third show indifferent changes and the last third a warming, then three distinct orthogonal functions are determined where members of the respective evolution have larger weights, as determined by the coefficients, for the respective EOF and lower weights to the other two.

Now, for each time step, the produced PCA components can be recombined to give new combinations of EOF and respective coefficients in as many ways as is necessary or wanted. Here, we choose to randomly resample the PCA components expanding the original matrix from 128 to 10000 members. The much larger number of data makes a statistical approach more elaborate and viable. Due to the orthogonality of the EOFs and the linearly independence of the coefficients, the statistics are not dependent on how the recombination is completed. In the last step of the process, the ensemble mean for each time step is added to the new ensemble, and finally the expanded ensemble is multiplied by the respective standard deviation.

During the recombination, the opportunity rises to make choices of the properties in the resulting ensemble. Often, a PCA-analysis is encouraged through its ability to reduce the dimensionality of the data set and get rid of noisy information. This puts a subjective perspective on the analysis that may put great emphasis on the users discussion of the choice of retained components and theirs justification. Conversely, in this study, it is of greater interest to evaluate as many climate scenario evolutions as possible, concerning both trends and variability, in trying to give a more complete analysis of the uncertainties in model simulations. In addition, the smaller contribution from the low-weighted components to the mean or variability can easily, though, be preserved in the new ensemble as their impact on the resulting set in itself are relatively moderate. Therefore, all the components are kept in the large ensemble in order to capture greater amount of information about the simulated climate characteristics in the 21st century.

Dettinger (2006) argues that due to differences between models in their component structure and configuration the PCA should be undertaken separately for each model and then append the new members into a corresponding ensemble matrix. Furthermore, the analysis can also be performed for a specific scenario or for ensemble mean vectors; however, to make an extensive evaluation, several forcing scenarios should be included as well as keeping the separate runs and thus preserve more of the natural variability in the models. In view of this, the PCA is computed for the AOGCMs separately including all available scenarios and members.

4. Results

4.1 Control climate (1961-1990)

Here we investigate the control climate in the AOGCMs for a smaller area; on national and sub-national scales. Emphasis is put in comparing the simulated climate for the control period (1961-1990) with observations on relevant spatio-temporal resolutions. First, we look at the large-scale circulation, which in large part governs the precipitation climate in Scandinavia, especially in winter, and to a certain extent the surface temperature. Secondly, we deal with the seasonal cycles of temperature and precipitation. For each AOGCM ensemble mean data calculated over all available ensemble members is used. Comparisons are made with partly model derived data; ERA40 reanalysis data (Uppala *et al.*, 2005) and also with a regional simulation with RCA3 forced with ERA40 on the boundaries (hereafter called RCA3ERA40). The observational dataset is the gridded CRU dataset. For further details on the evaluation data see section 2.3.

4.1.1 Mean sea level pressure

The AOGCMs, in general, successfully simulate the winter mean sea level pressure (MSLP) patterns over Europe, although the strength of the westerlies differs quite significantly between the models. In IPCC (2007), the MSLP fields over Europe are compared with NCEP (Kalnay *et al.*, 1996) reanalysis data. Instead of evaluating each model they use the ensemble mean of all AOGCMs, and the resulting pattern indicates a somewhat too weak north-south pressure gradient. This leads to a weaker than observed westerly flow over the northern parts of Europe (Christensen *et al.*, 2007). We compare the multi-model mean with the ERA40 reanalysis and the results show, similarly, a too weak north-south pressure gradient in the northern parts of the European region (Fig. 4.1). However, the variability and spread among the models is significant with some models (*e.g.* CCSM3 and HadGEM1) showing a too strong north-south pressure gradient while others (*e.g.*, CSIRO-MK3.0 and GISS-ER) show a too weak north-south pressure gradient more in line with the multi-model mean.

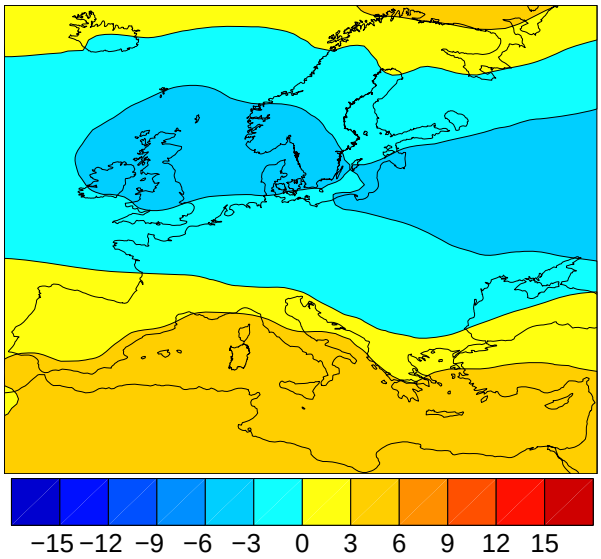

Figure 4.1. *Multi-model mean winter (DJF) bias of the mean sea level pressure (MSLP) compared to ERA40 data for the control period 1961-1990. Units are in hPa.*

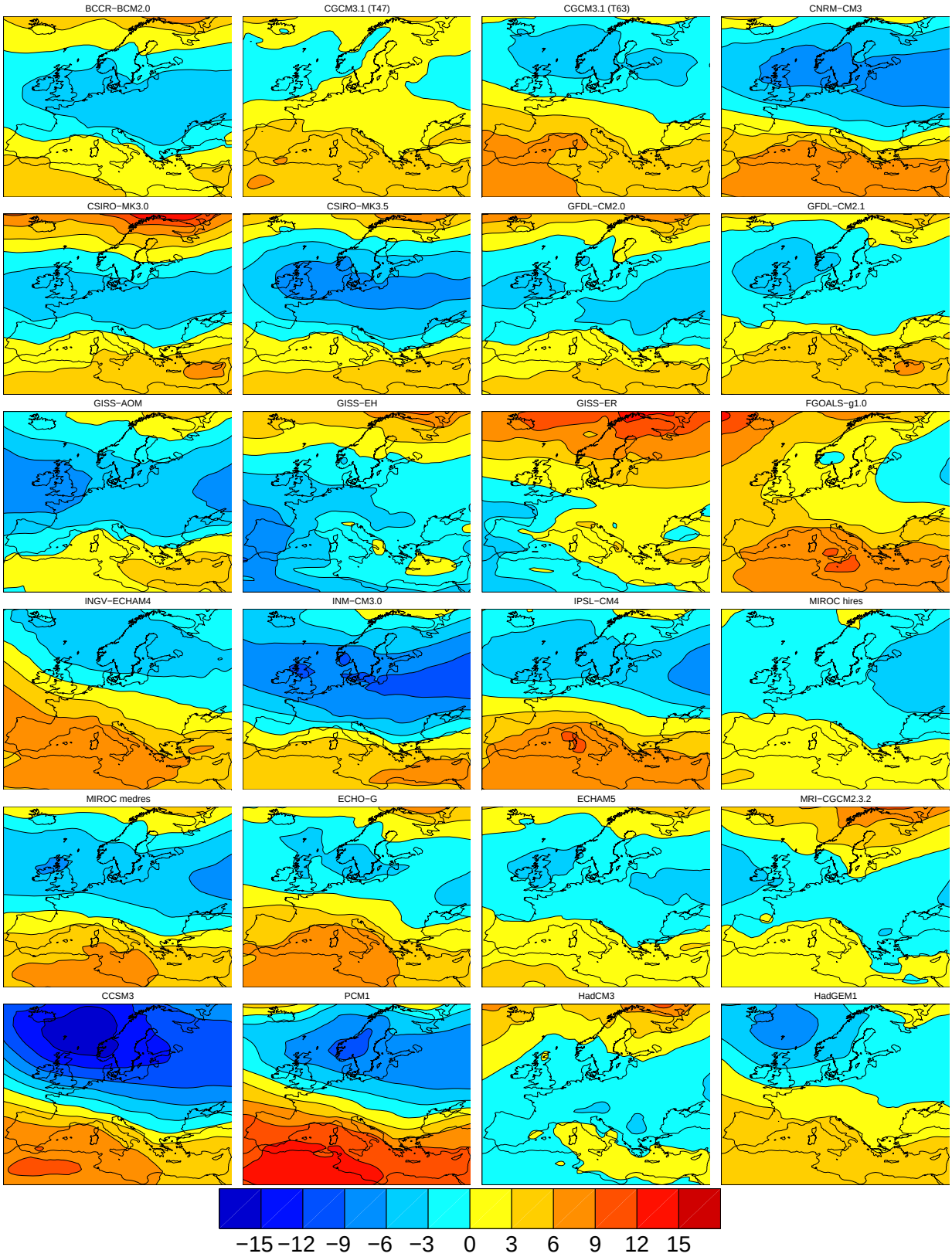

Figure 4.2. *Winter (DJF) MSLP difference in the 1961-1990 mean between AOGCMs and ERA40. Units are in hPa.*

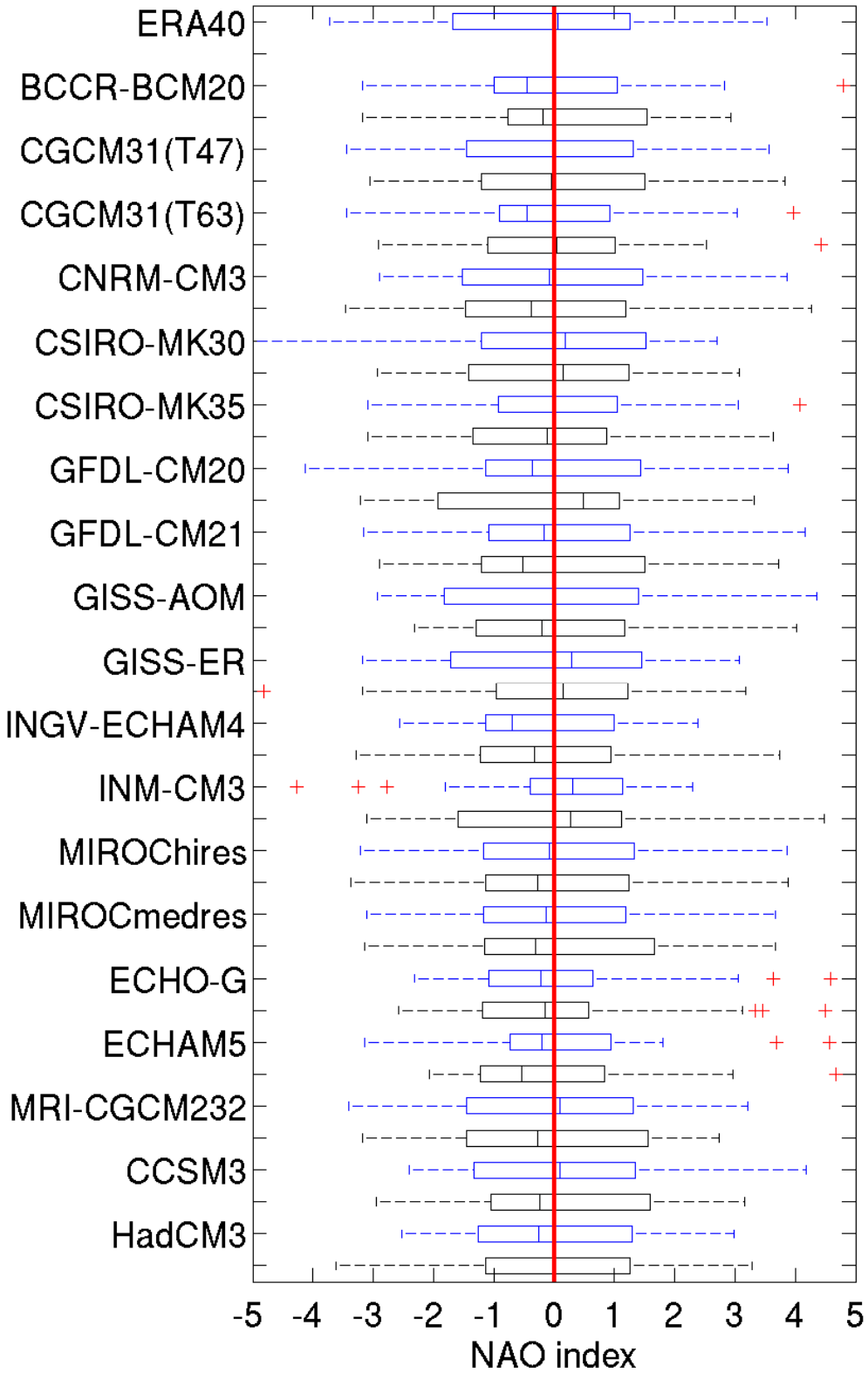

Figure 4.3. *Box diagrams of normalised winter (DJF) NAO index for 1961-1990 (black boxes) and for 2071-2100 in the A1B scenario (blue boxes). Positive values represent positive NAO phases with stronger north-south pressure gradient. The vertical line in each box represents the mean of the 30 winter seasons and the boxes constrain the upper and lower quartiles, and thus give the middle 50%. Dashed lines give the extent of maximum and minimum values and the red markers are outliers (that are more than 1.5 times the interquartile range outside of the box). The red solid vertical line represents the zero line.*

To further condense the information of the effects of the large-scale pressure field on the climate in northern Europe, an analysis of the normalised winter NAO-index (Hurrell, 1995) has been performed for the models (except FGOALS), for both the control period (1961-1990) and the 2071-2100 period under the A1B scenario. The results are represented by a box-plot that describes the distribution of the index. Included is also ERA40 data for the 1961-1990 period. As Fig. 4.3 shows for the control period, there is no systematic bias in the winter NAO in any of the AOGCMs, although most models tend to have a somewhat lower mean value (*i.e.* too weak north-south pressure gradient). The inter-annual variability is large and both positive and negative phases of NAO occur regularly as depicted by the boxes (the region constrained by the lower and higher quartiles, representing the middle 50%) in both models and observations. A few models display asymmetries around the mean (and the zero line); for example BCCR BCM2.0 has a mean somewhat below zero with a distribution skewed towards larger positive values in the central part of the probability distribution. This property is evident also for CCSM3, GFDL CM2.1, MIROC (medres and hires) and MRI CGCM2.3.2. However, the effects of these biases in the pressure fields are not clearly discernible in simulated precipitation and temperature in the control period: even though AOGCMs typically simulate winter precipitation rates above the ERA40 mean, particularly in the south, it is common in almost all models, with no distinction between them that can be clearly attributed to the circulation. Furthermore, the temperature field shows a cold bias among the majority of the models, which in the general case could be explained by the weaker north-south gradient if taking the mean of all models (Fig. 4.1). However, the models mentioned above, with large spread into the positive phase, do not exhibit warmer climates than the others.

4.1.2 Surface temperature

The surface temperature is dependent on several factors, one of them the atmospheric circulation and thereby winds in lower levels. In winter the strength of the westerlies modifies the temperature by bringing more or less moist and mild air masses from the North Atlantic in the west. Both in the northern and southern part of Sweden, the winter temperature, averaged over the time period 1961-1990, clearly shows a general cold bias among the AOGCMs compared to ERA40 (Fig. 4.4). As discussed earlier, the models seem to underestimate the north-south pressure gradient (i.e. the multi-model mean in relation to NCEP and ERA40 reanalysis) that suggests weaker westerlies and thus colder conditions over northern Europe. The Chinese FGOALS model is much too cold in all seasons, most notably during winter when it simulates a climate close to that of the Last Glacial Maximum for this region (Kjellström *et al*., 2009). In the following analysis of climate change we have excluded that model as it is too unrealistic in the control period. Not all models display a negative temperature bias; the Japanese MIROC 3.2 (high-resolution version) tends to have a small positive bias of around 1-2°C in both the north and the south of Sweden, most evident in summer and in the south where it is higher throughout the year. Furthermore, while most of the models tend to have similar biases in all months varying not more than 2-3°C, some display seasonal patterns in the deviations from ERA40 (see Fig. 4.4). For example, in southern Sweden, ECHO-G display a quite distinct bias pattern over the seasons; a warm bias of around 4°C in winter, while in summer the model has a negative bias being some 7°C colder in June compared to ERA40. The result indicates a significantly weaker seasonal cycle in the ECHO-G model, which could partly be explained by the land-sea resolution in the model (cf. Fig. 2.2). Conversely, the BCCR-BCM 2.0 has a cold bias in winter of approximately 8°C and a warm bias in summer (1-2°C above the ERA40 line), which in this

case points at a clearly stronger seasonal cycle than observed. The same models show the same pattern in northern Sweden as well, although the seasonal cycle in ECHO-G is not as much weaker as in the south.

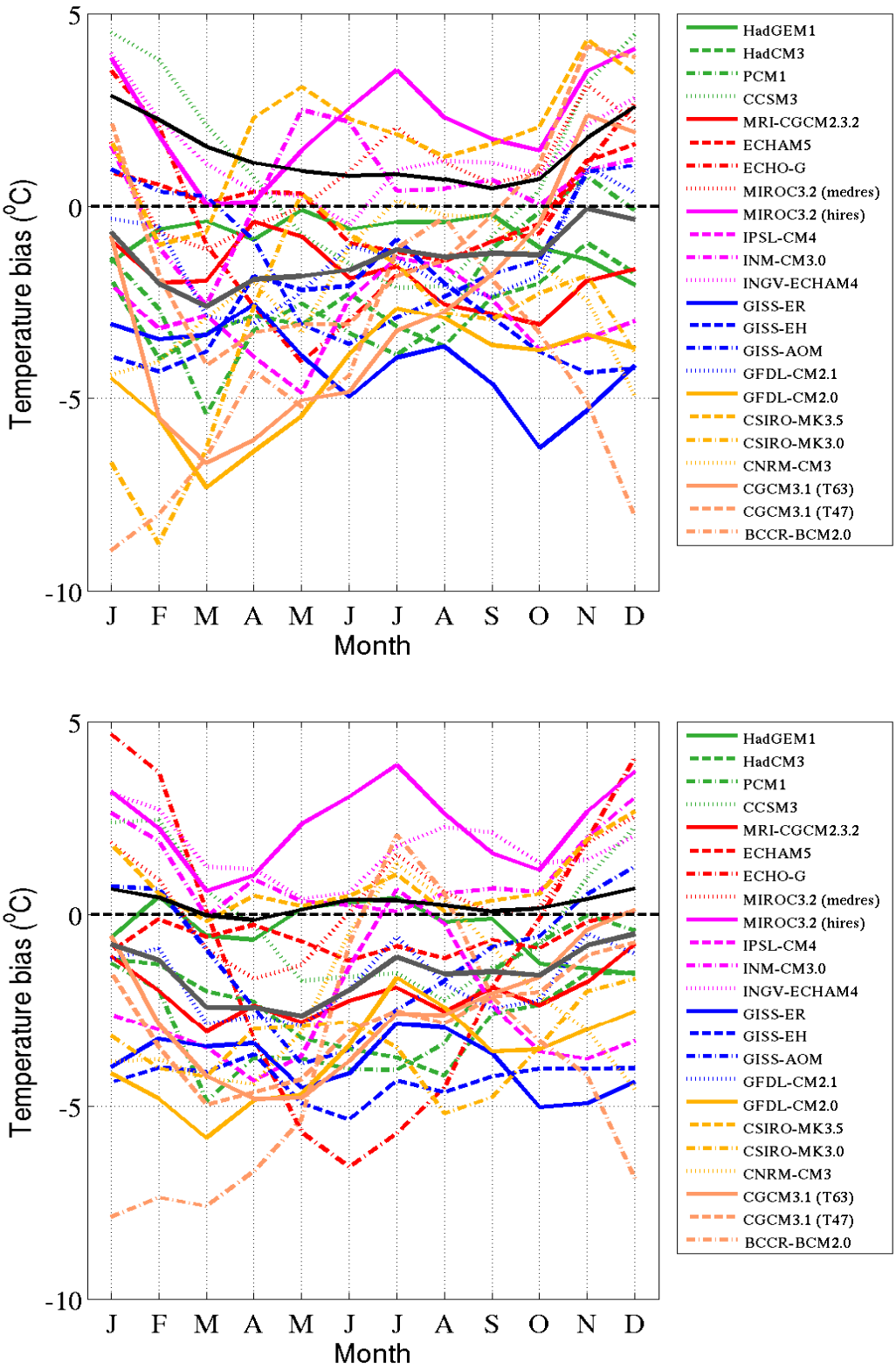

Figure 4.4. *Seasonal cycle anomalies of 2m-temperature compared to CRU TS2.1 in 1961-1990 for northern (top) and southern Sweden (bottom). The solid black line represents ERA40. Solid grey line represents the AOGCM multi-model mean difference. Units are in °C.*

A few models show a seasonal cycle of temperature that deviate not more than 2-3°C from the observations. In the north, INGV-ECHAM4 agrees better with ERA40 than any of the other models. In the south, INGV-ECHAM4, CCSM3, MIROC 3.2 (medium res.), HadGEM1, ECHAM5, INM-CM3 and CSIRO MK-3.5 all exhibit a better agreement than the rest, within +/- 2-3°C, especially in summer. These models agree better with ERA40 also in the north, except for HadGEM1 and INM-CM3.

It is in place to mention something about the uncertainties in the observations. All observations are associated with some degree of uncertainty. In that regard, when using observational data sets for evaluation, one should always bear in mind the known quality and deficiencies of the data. This is more thoroughly discussed and examined in Lind and Kjellström (2009), looking at precipitation and temperature in the Baltic Sea runoff area. Concerning the two data sets, which are used in this report, CRU is generally colder than ERA40. The difference between the two datasets is up to 2-3°C in northern Sweden during winter (Fig. 4.4) implying a better agreement between models and CRU in general. In southern Sweden differences between ERA40 and CRU are small throughout the year. In winter the bias amounts to around 2-3°C (within +1°C in INGV-ECHAM4) and 1-2°C during the rest of the year (+/-1°C in the average).

4.1.3 Precipitation

Due to the significant heterogeneity of humidity and dependence of precipitation processes on local characteristics, AOGCMs face a major challenge in capturing the spatio-temporal pattern as well as the maximum and minimum values on the regional or smaller national scale, like Sweden.

The spread of the models in the seasonal cycle of precipitation in both regions in Sweden is quite significant (Fig. 4.5). There is an overall tendency to overestimate precipitation in both the north and the south compared to ERA40. This is true for all months except in summer when most of the AOGCMs display lower values compared to both ERA40 and CRU, and especially compared to RCA3ERA40.

In the north, few AOGCMs accurately capture the seasonal cycle; most of them have the yearly maximum in the autumn or early winter, whereas in ERA40 (and in CRU and RCA3ERA40) the maximum occurs during summer. Exceptions are the GFDL-models, MRI-CGCM2.3.2, ECHAM5, HadGEM1, CNRM-CM3.0 and MIROC3.2 (medium resolution) that succeeds reasonably well in capturing the phase. The CNRM model has a strong cycle with the summer maximum well above all the other models and ERA40, reaching nearly 120 mm/month in July. Some models, for example the GISS-EH, ECHO-G and FGOALS models have a minimum in summer instead of a maximum.

In the southern part of Sweden, the AOGCMs generally simulate more precipitation in winter, spring and autumn, compared to ERA40, while in summer there are some models having less precipitation than ERA40. Again, a few simulates a minimum in summer which, in contrast, is observed to appear in late winter or spring, see for example ECHO-G, IPSL-CM4 and FGOALS.

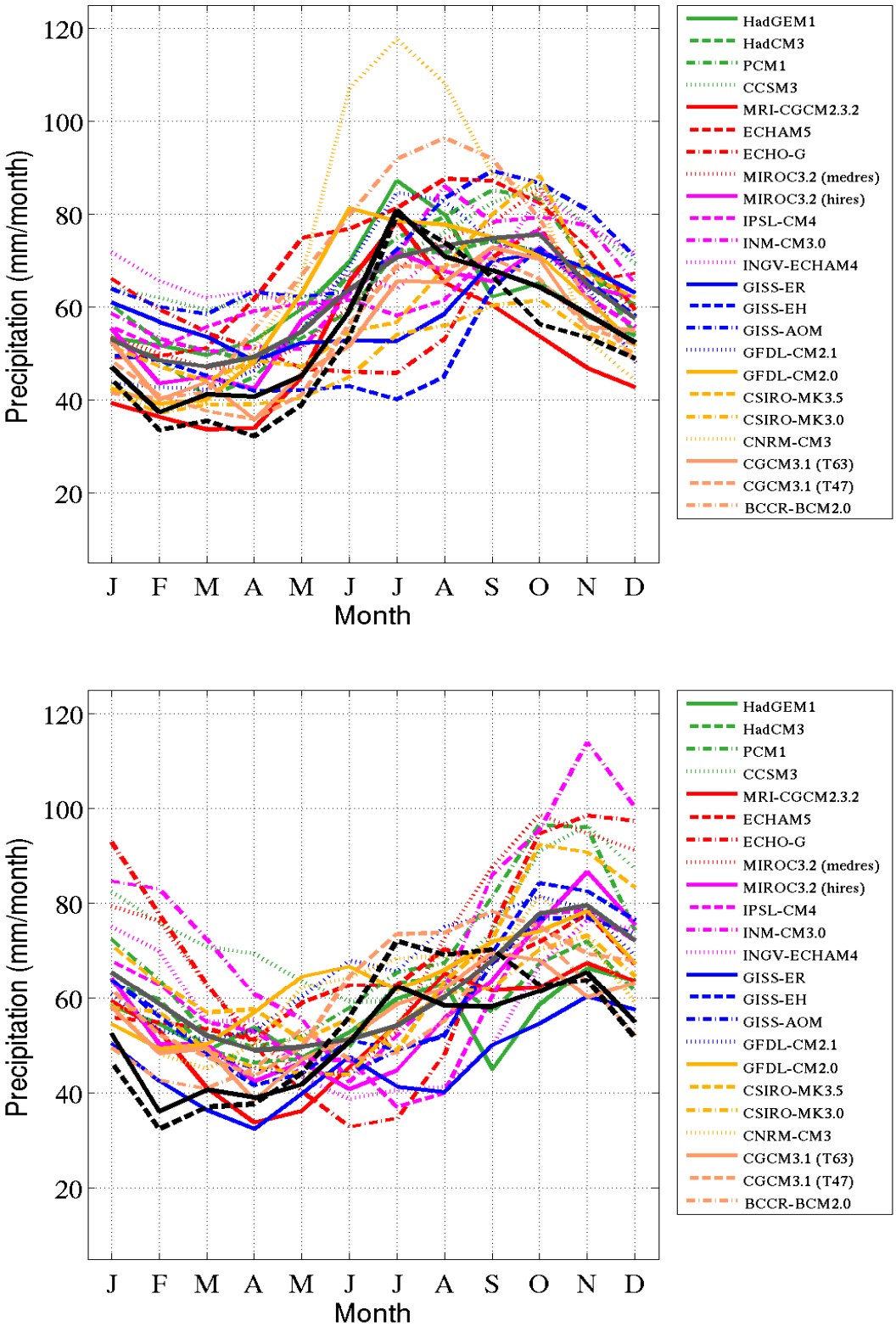

Figure 4.5. *The AOGCM simulated seasonal cycles in precipitation in the base line period between 1961 and 1990 in northern (top) and southern (lower) Sweden. Black solid, dashed and dash-dotted lines are ERA40 and CRU respectively. Solid grey line is the AOGCM mean. Units are in mm/month.*

All in all, the AOGCMs seem to produce too much precipitation in Sweden, both in the north and the south, except in summer. In addition, the seasonal cycle differs among the models and the spread is large, where some capture the phase and magnitude fairly well (MRI-CGCM2.3.2) and others misses completely the minimum and maximum (*e.g.* FGOALS and ECHO-G). As expected, the agreement between AOGCMs on the one hand and reanalysis and observation data (ERA40 and CRU) on the other is weaker for precipitation than for sea level pressure and surface temperature on the regional scale. Deviations of around 30-40 percent are not uncommon, a significant bias that should be borne in mind when studying climate change signals.

The geographical details in the simulated precipitation are generally in better agreement with observations in the regional climate model than in the corresponding AOGCMs. This better agreement has been shown to be particularly noticeable in high-altitude areas as the Scandinavian mountain chain by Rummukainen *et al*. (2001) for an earlier version of RCA. Such an improvement is a result of the higher resolution and thereby better description of land-sea contrasts (cf. Fig 2.2) and orography (not shown). Rummukainen *et al*. (2001) also show generally decreased biases for seasonal mean temperature and precipitation compared to observations for their entire model domain in northern Europe. Kjellström and Lind (2009) show that forced with two different AOGCMs, also RCA3 is better at reproducing the phase of the observed seasonal cycle over the Baltic Sea catchment area in the control period than the corresponding AOGCMs themselves. On the contrary, they show that, the amount of precipitation is more overestimated in RCA3 than in the AOGCMs during summer.

4.1.4 Combined precipitation and temperature

Another way to highlight biases in the simulated recent climate in the models is to combine precipitation and temperature in scatter diagrams, and, in addition, include several members of the same AOGCMs separately (i.e. no ensemble mean are used). AOGCMs with only one single run are excluded from this analysis. By incorporating the observed (CRU and SMHI) tri-decadal values in the diagrams, not only the general bias in the AOGCMs can be investigated but it also enables a comparison of the spread between the members in a single model in relation to the decadal variability represented by the spread of the observational data.

Fig. 4.6 shows scatter diagrams for winter in the northern and southern part of Sweden. All data are given as anomalies, in °C for temperature and % for precipitation, compared to the SMHI record for the time period 1961-1990. When comparing precipitation it is worth noting that a % difference in summer will be significantly larger than the same % difference in winter in terms of absolute values.

Four AOGCMs have been selected to highlight the biases and spread among members, indicated by coloured symbols; GISS-ER (9 members), CCSM3 (8 members), CGCM 3.1 (T47) (5 members) and ECHAM5 (4 members). In the north, the precipitation bias in the two former models is large, around 50-60% above observations in the mean. As one moves to the south this bias is still seen in CCSM3, while in GISS-ER the bias is practically absent. As was clarified earlier, most of the AOGCMs have too much precipitation in the control period (1961-1990) in winter in the whole of Sweden, clearly seen in Fig 4.6. The temperature climate varies, as well, significantly between the models; biases spans from around +4°C to -8°C. However, there is a weight towards too cold conditions in most models as noted earlier.

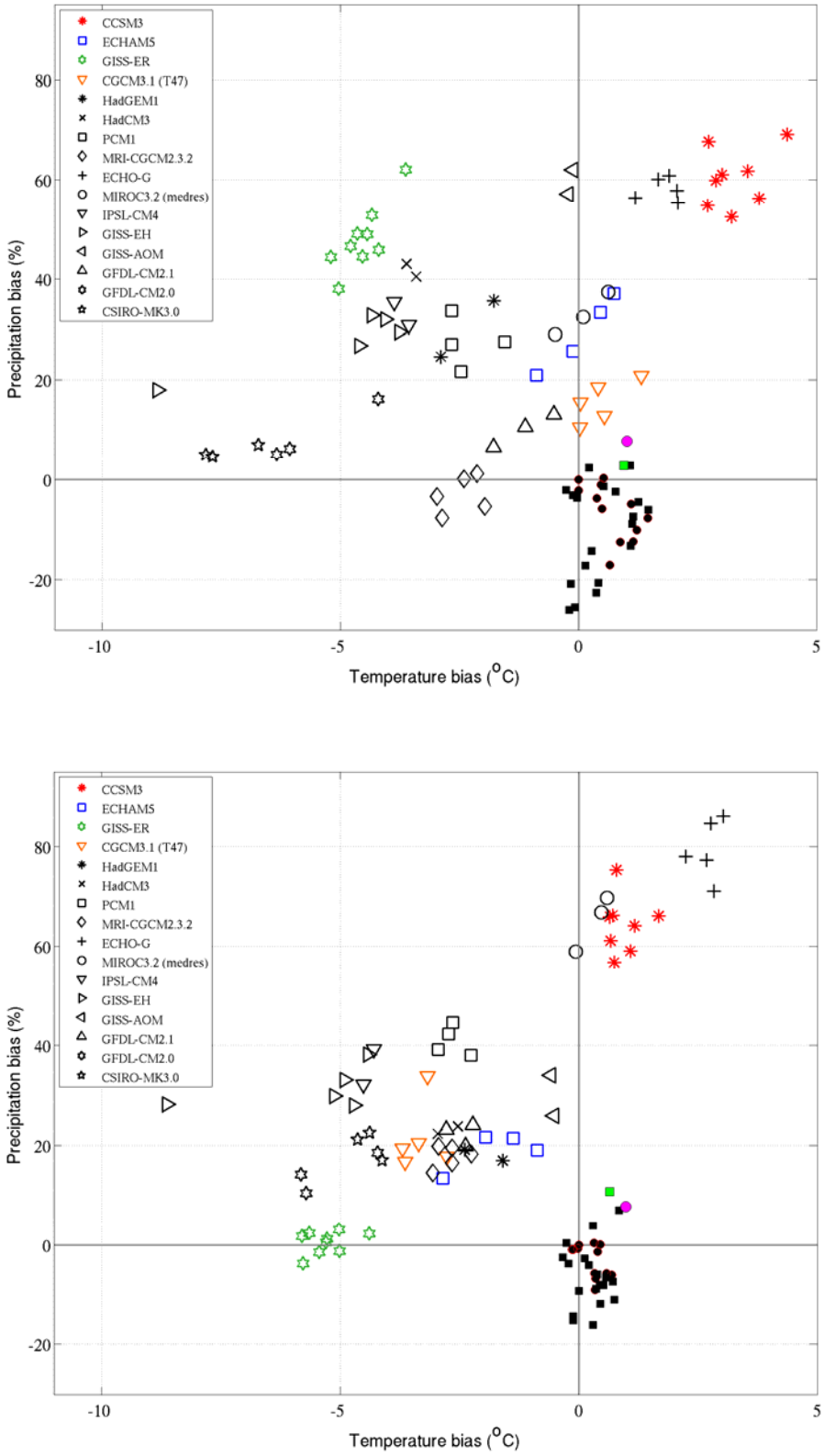

Figure 4.6 *Scatter diagram of winter (DJF) 2m-temperature and precipitation biases for northern (top) and southern (lower) Sweden in the years 1961-1990. The black squares and circles represent the SMHI and CRU observations respectively. The filled green square and magenta circle are the latest observed tri-decadal mean. See text for further details.*

What is further interesting is the spread among the individual members in an AOGCM. The observed 20th century climate demonstrates a span of around 30% for precipitation and around 2°C for temperature (a little lesser in south). In the north, the members of GISS-ER have a spread that spans not more than 25% in precipitation and around 2°C in temperature. This is true also for the other highlighted AOGCMs and even for the entire assembly of models. An exception is GISS-EH where one of the five members has a drastically lower temperature; the outlier is some 4°C colder than the rest of the group. The clustering of the members is similar in south, with no radical spread that exceeds the observed decadal variability (GISS-EH still an exception).

In summer (Fig. 4.7) the precipitation bias shows both positive and negative signs, with more weight towards negative bias in southern Sweden. All models have a colder climate than the SMHI data, except MIROC 3.2 (medium resolution), which show a close agreement with observations, especially in the north. The span in the observed record amounts to around 15-20% in precipitation and 1°C in temperature in both areas. ECHAM5 has a small spread in temperature for the two regions (less than 0.5°C) and 10-15% spread in precipitation. GISS-ER has somewhat larger deviations in temperature of around 1°C. However, this model also has a larger ensemble, which in principle should increase the spread. In the south CCSM3 has two distinct groups of members, separated by around 10% in precipitation bias. All in all, the span between ensemble members of the AOGCMs is again generally similar to the observed decadal variability.

This analysis indicates that multiple member runs can represent the observed decadal variability. However, the SMHI and CRU records constitute a relatively short period of time and are also influenced by the anthropogenic activities, and thus do not solely represent natural variations. Again, the sizes of the ensembles come into play here. Even though the spread is not overwhelmingly large, so are not the ensembles as well. Therefore, with larger ensembles the spread should increase somewhat.

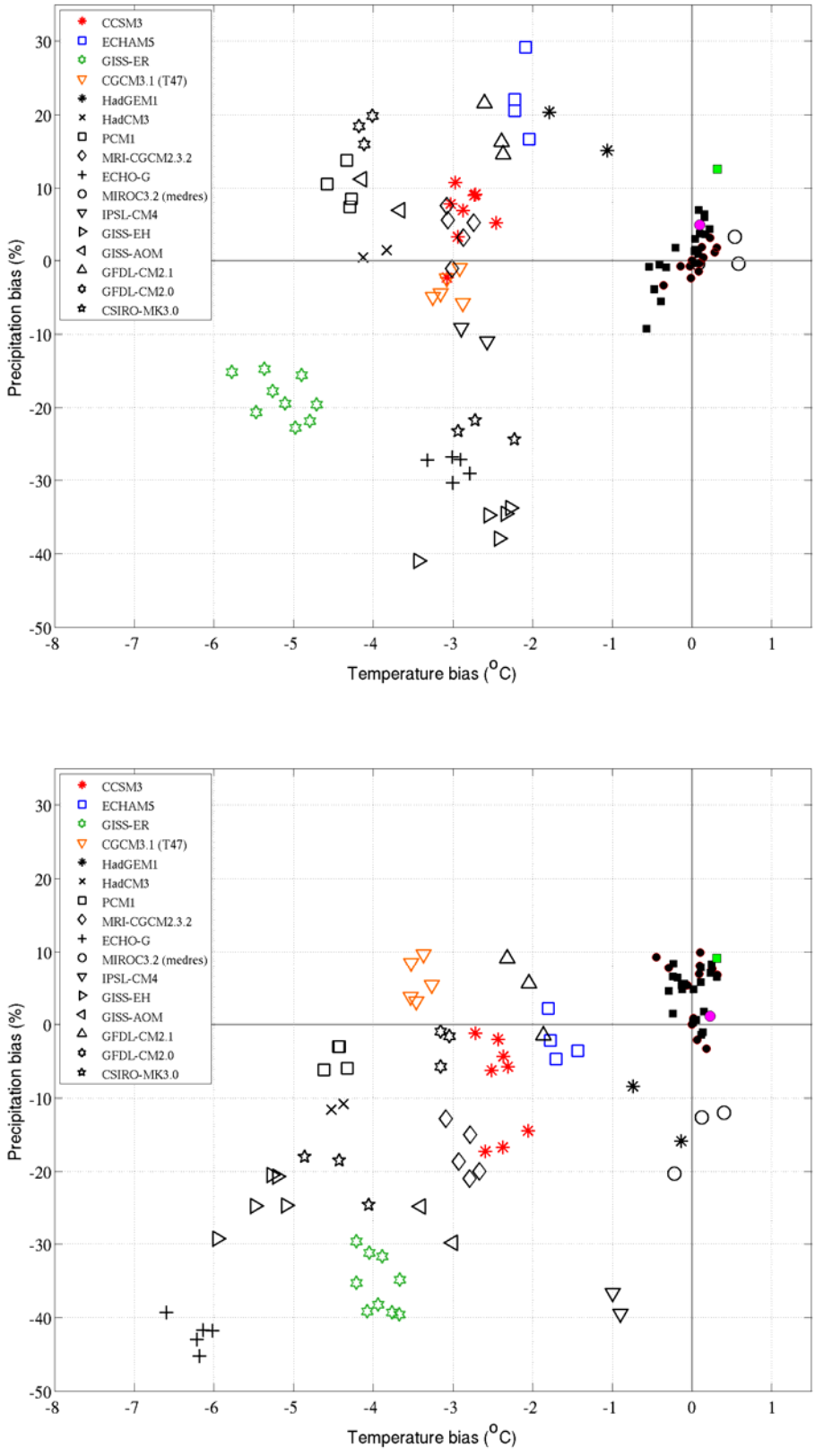

Figure 4.7. *Scatter diagram of summer (JJA) 2m-temperature and precipitation biases for northern (top) and southern (lower) Sweden in the years 1961-1990. The black squares and circles represent the SMHI and CRU observations respectively. The filled green square and magenta circle are the latest observed tri-decadal mean. See text for further details.*

4.2 Transient climate change in the 21st century in Sweden

In this chapter, the climate change signals from the AOGCMs used in IPCC (2007) are analysed with respect to temperature and precipitation for the southern and northern part of Sweden in an effort to give a more complete representation of potential climate changes. Along with this, the responses from the regional climate models are included, with the aim to compare and relate the results from global models with downscaled data.

4.2.1 Changes in the large-scale circulation

In IPCC (2007), the north-south pressure gradient is found to increase in the 21st century, although with large spread between the models. The reason for the increase is a projected decrease in Arctic pressure and an increase in mid-latitude and sub-tropical pressures, giving a northward shift in the mid-latitude storm track (Fig. 4.8). Projections of the NAO index by the end of the 21st century show distributions where the mean is higher (more positive/less negative) than in the control period, *i.e*. stronger N-S pressure gradient, in 13 out of 19 AOGCMs (Fig. 4.3). This increase in the NAO index indicates stronger westerlies on average. This is consistent with the study by van Ulden and van Oldenborgh (2006) who analysed projected changes in precipitation and temperature for a region in central Europe. They partly attributed increases in both these variables to an increase in the westerly flow, especially in winter, the rest being due to thermodynamical effects. However, we note that a direct comparison with the results from van Ulden and van Oldenborgh is not clear-cut. The reason is that their results are based on partly different data sets, as they do not use exactly the same set of AOGCMs used here.

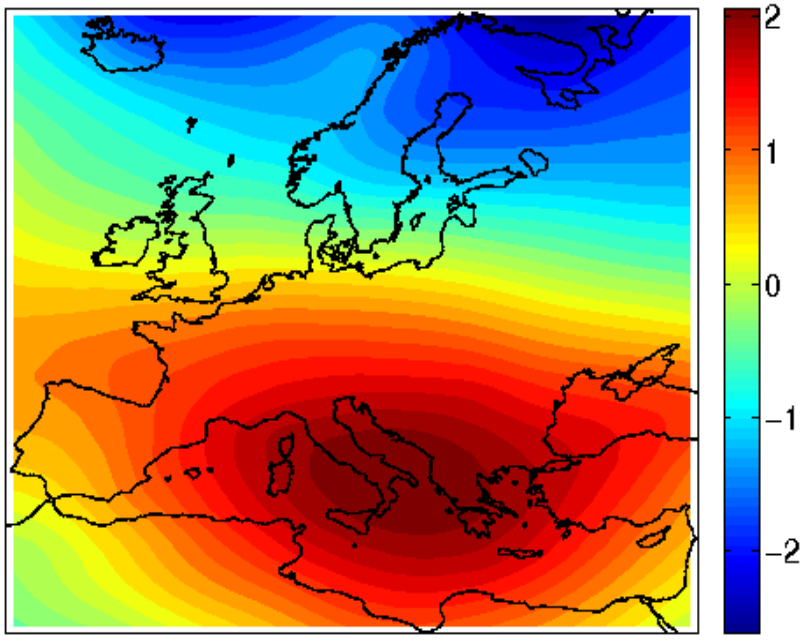

Figure 4.8. *The simulated multi-model mean change of the winter (DJF) mean sea level pressure (MSLP) between the control period 1961-1990 and the end of the century, 2071-2100, under the A1B scenario. Units are in hPa.*

4.2.2 Changes in seasonal cycles

By the end of this century, all AOGCMs project an increase in 2m-temperature in all months both in the north and in the south and for all scenarios (Fig. 4.9 showing the A1B scenario). The seasonal changes show the largest increase in winter and smallest in summer. The minimum in summer is, however, not distinct in all models; some instead have similar changes in autumn and spring. The change in July, for example, varies between around 1 and 5.5°C. In the southern region, this seasonal pattern in the signal is less pronounced; in MIROC3.2 (high-resolution) the temperature increase fluctuates not more than around a half degree throughout the year from its mean positive anomaly of approximately 5°C. The Norwegian BCCR-BCM 2.0 model shows a strong signal in winter; this is possibly due to a too cold control period (see Fig. 4.4).

Considering precipitation in the A1B scenario, the seasonal changes for Sweden are not especially coherent between the AOGCMs even for the later period (2071-2100), see Fig 4.10. The spread is some 30-50%. For the summer season not even the sign of the change is uniquely determined in the south. The AOGCMs simulate changes varying between around -30 and +40%, with approximately the same number of models on each side of the non-change line. The consensus increases in autumn and also for the stronger forcing in the A2 scenario (not shown). In the north, there is a general agreement of a positive signal in all months, except for summer where a couple of models indicate a smaller decrease.

To conclude, the AOGCMs have similar seasonal changes by the end of this century for the surface temperature, while the spread is considerable for precipitation. However, as been noted earlier (*e.g.* Christensen *et al.,* 2007), the large-scale climate change signal in precipitation is coherent in all AOGCMs with increasing precipitation in northernmost Europe and decreasing precipitation in the south. It is only the border line between increasing and decreasing precipitation that differs. This difference has a profound impact on the uncertainty in projections of summertime precipitation in southern Sweden as shown in Figs 4.10

We also note that the climate change signal in the seasonal cycle may be influenced by the natural variability. Seasonal means may differ with about 0.5°C in temperature or 10% in precipitation between single ensemble members as indicated in Figs. 4.6-4.7. When combined into a climate change signal between two periods this may lead to differences in 1°C and 20% between two climate change experiments. Further, if these differences act in different directions for summer and winter a total difference in the amplitude of the seasonal cycle may end up at 2°C or 40%. Such large potential differences between ensemble members must be kept in mind as a major source of uncertainty in the climate change signal, especially in the nearest few decades when the climate change signal is still moderate. However, by using the ensemble mean for each model the noise should be reduced substantially.

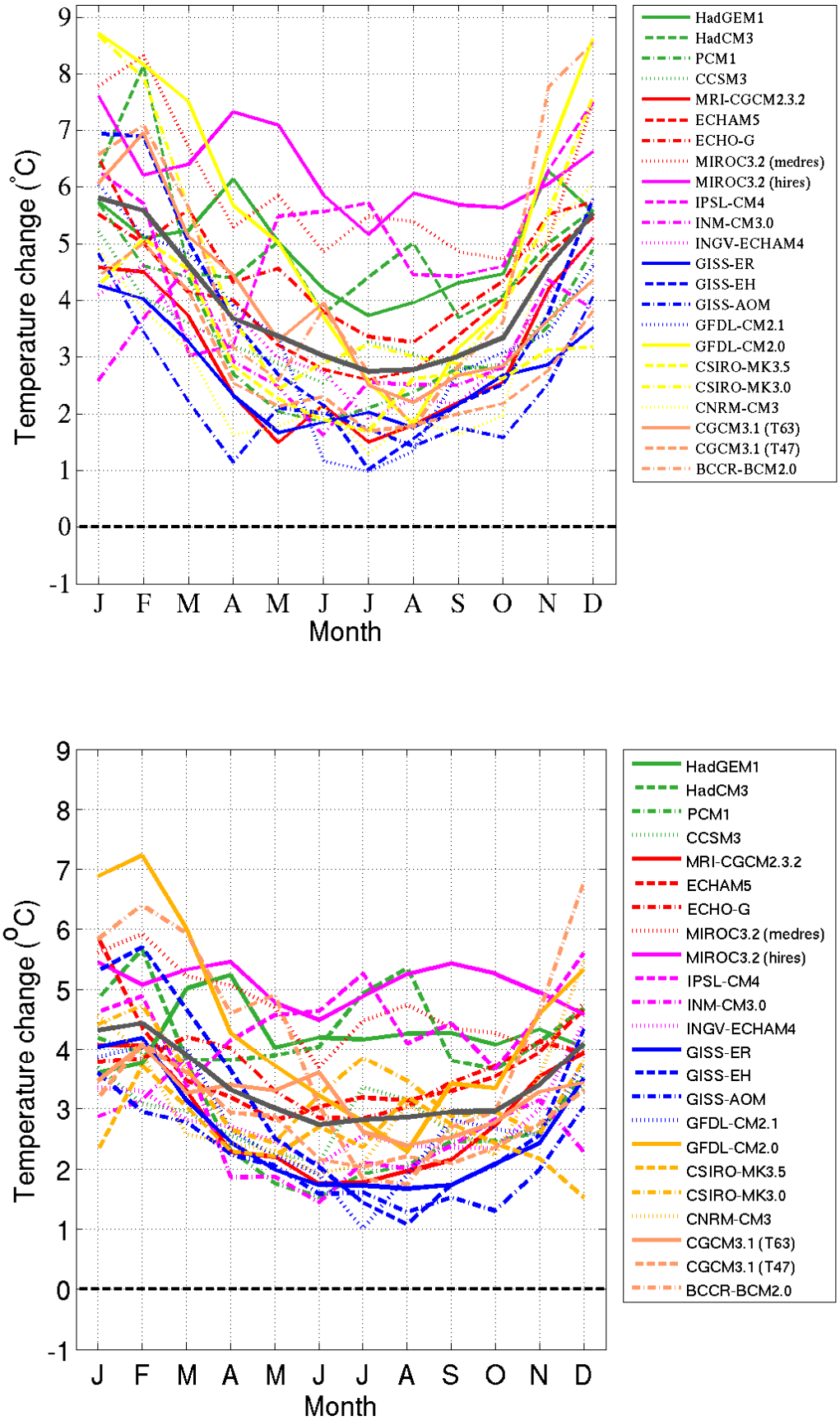

Figure 4.9. *Seasonal cycle of monthly mean changes in 2m-temperature under the A1B scenario by the end of the 21st century (2071-2100) in northern (top) and southern (bottom) Sweden. Solid grey line depicts the AOGCM multi-model mean changes. Units are in °C.*

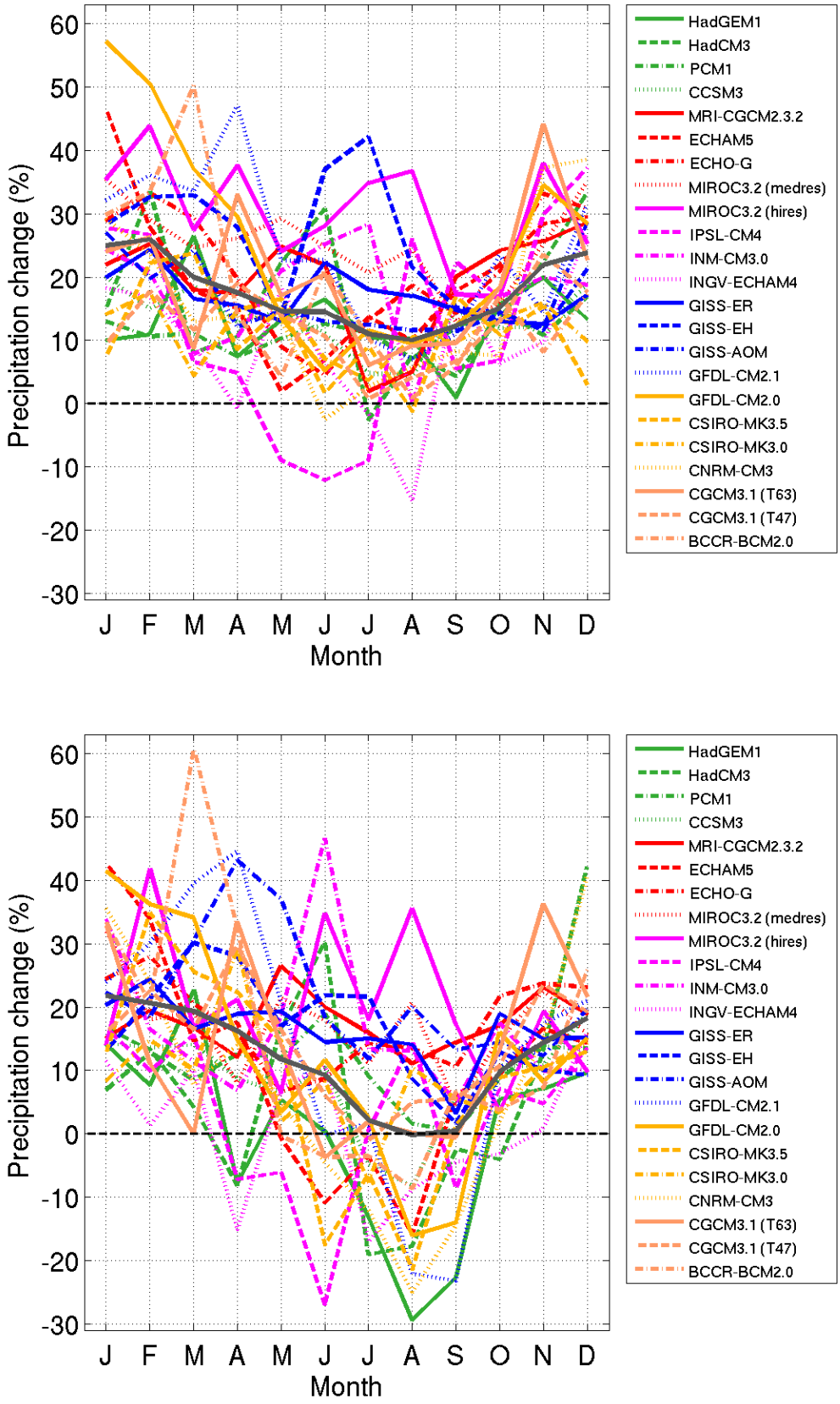

Figure 4.10. *Seasonal cycle of monthly mean changes in precipitation under the A1B emission scenario by the end of the 21st century (2071-2100) in northern (top) and southern (bottom) Sweden. Solid grey line is the AOGCM multi-model mean. Units are in %.*

4.2.2 Scatter-plots; individual scenarios and multi-scenario analysis

In all seasons, a significant change in temperature can be seen already in the near future, in the 30-year mean for 2011-2040 (Fig. 4.11), i.e. temperature values are well above the observed decadal variability. Also in the case of precipitation, more or less distinct signals of increases are seen in all seasons in both regions. An exception is summer, where precipitation changes are of the same order as 20th century decadal variability and not distinctly separated from the no-change line. In the near future, the different forcing scenarios are essentially indistinguishable as expected. On the longer time scales, when the forcing becomes stronger, the differences become more obvious (Fig. 4.12).

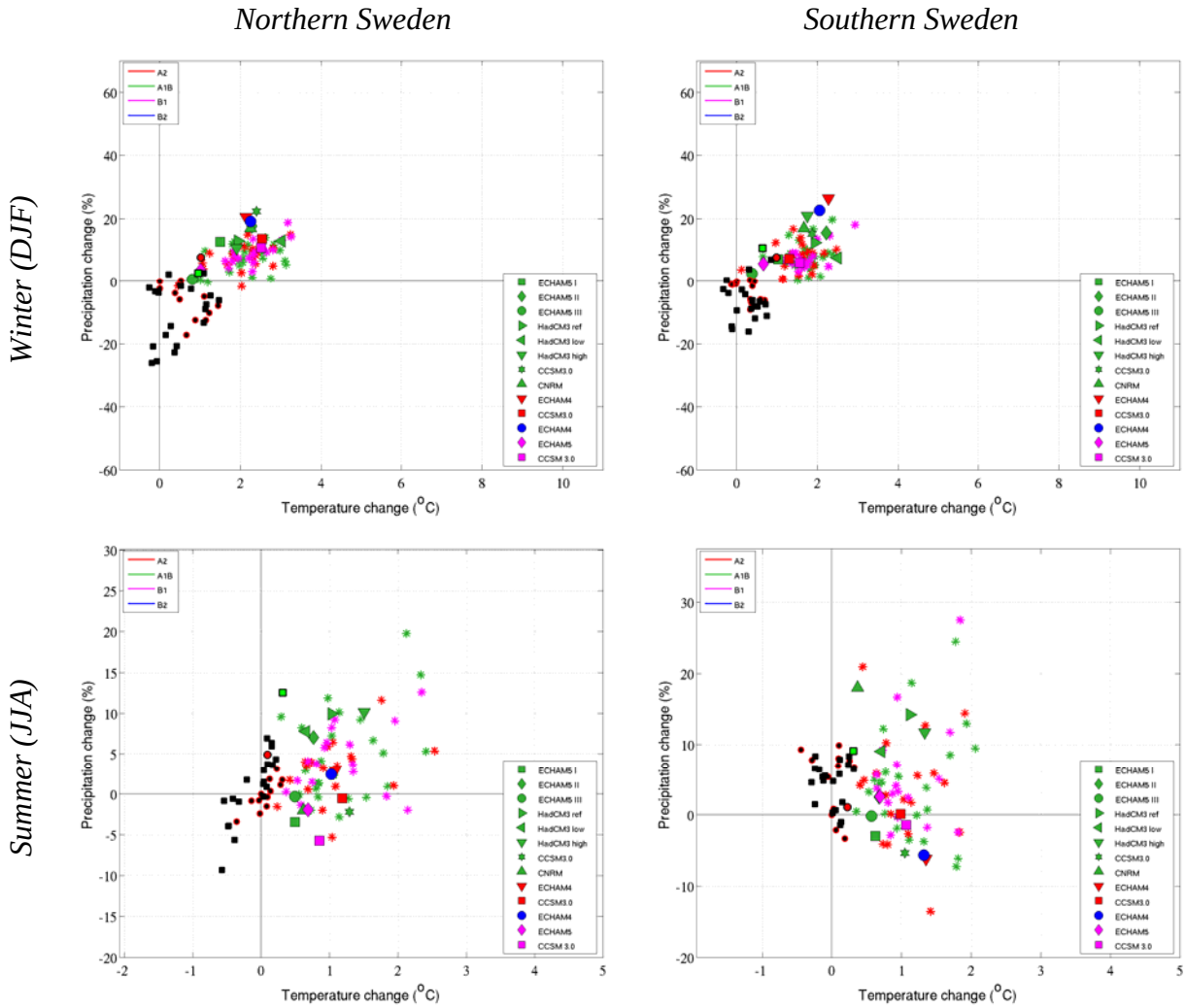

Figure 4.11. *Scatter diagram showing simulated 2m-temperature and precipitation changes in 2011-2040 compared to 1961-1990 for northern (left) and southern (right) Sweden in winter (DJF, top) and summer (JJA, bottom). Also shown is the 20th century variability as recorded by the SMHI (black squares) and CRU (black circles) observations respectively. The filled green square and red circle are the latest observed tri-decadal mean. The stars (*) denote the GCMs with colouring according to the upper left legend. The same colour scale applies to the right legend showing the RCA3 experiments with labels according to forcing GCM.*

Most regional climate model runs in the 2011-2040 period are close to the major part of AOGCMs for surface temperature (Fig 4.11). Also for the RCMs the differences between different emission scenarios are difficult to distinguish from each other. In the RCA3 runs

driven by ECHAM5 under the A1B scenario the changes are more moderate compared to the changes in the ECHAM4 driven A2 and B2 scenarios, which indicates that the uncertainty connected to the choice of driving AOGCM is greater than the uncertainties in the emission scenarios on this time horizon. Also, the downscaling of HadCM3 results are interesting in this respect as the HadCM3 (low) shows a stronger temperature change in the north than does the HadCM3 (high) despite the fact that the latter is more sensitive to the change in radiative forcing. The precipitation in summer in the RCA3 runs do not show significant climate change signals, i.e. well above or below observed decadal variability. In the south summer estimates are represented on both the negative and positive side, whereas in the north all the runs display an increase, however, within the observed variability. In the cold season, on the other hand, distinct signals are apparent, as with the AOGCMs. For instance, increases of around 20-30% compared to the reference period are seen in the RCA3 ECHAM4 and RCA3 CCSM3 runs.

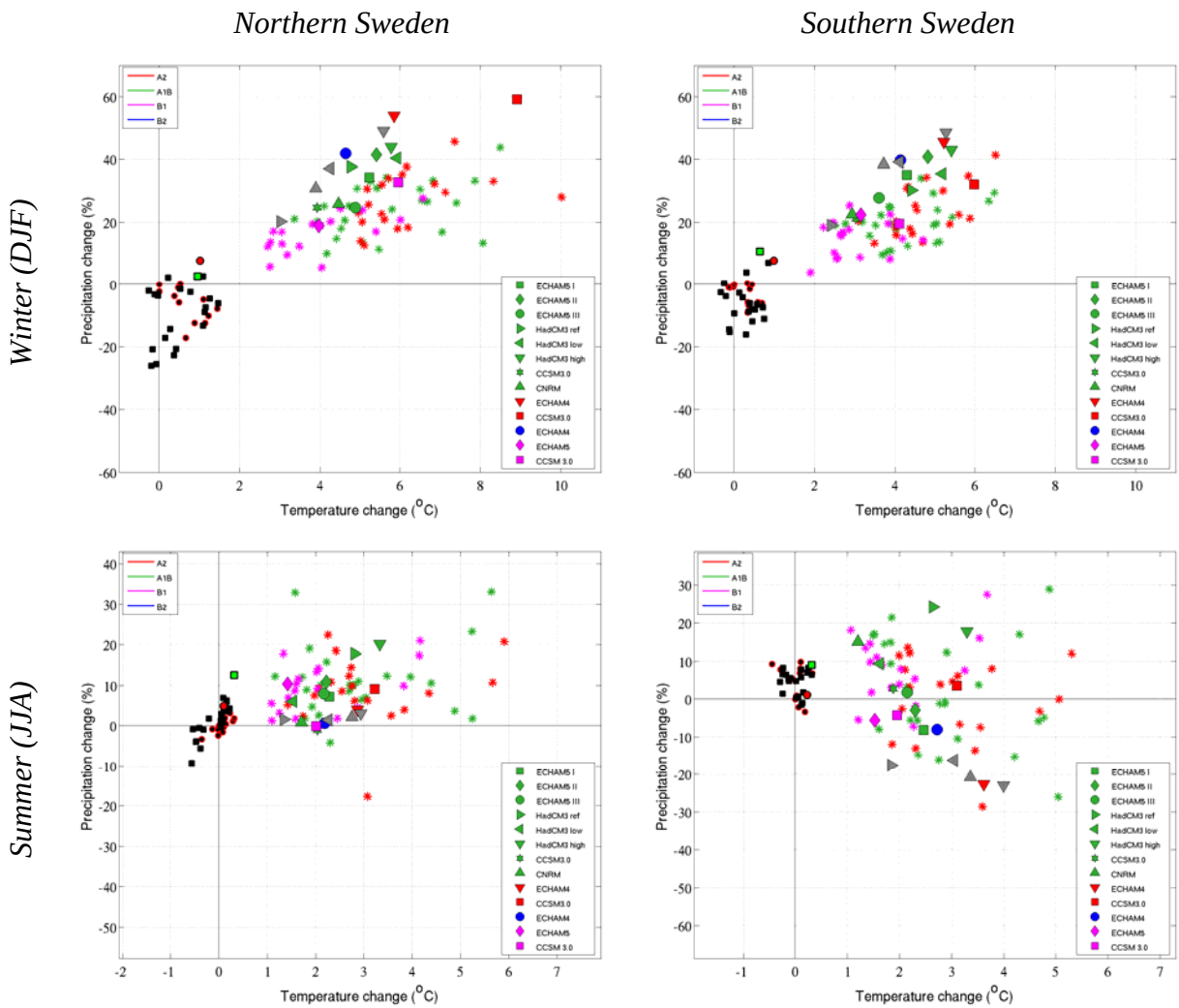

Figure 4.12. *Scatter diagram showing simulated 2m-temperature and precipitation changes in 2071-2100 compared to 1961-1990 for northern (top) and southern (lower) Sweden in winter (DJF, top) and summer (JJA, bottom). Also shown is the 20th century variability as recorded by the SMHI (black squares) and CRU (black circles) observations respectively. The filled green square and red circle are the latest observed tri-decadal mean. The stars (*) denote the GCMs with colouring according to the upper left legend. The same colour scale applies to the right legend showing the RCA3 experiments with labels according to forcing GCM. The grey symbols represents the four climate change experiments with RCAO.*

Moving forward in time, the pattern of the responses gradually becomes more unambiguous, and by the end of the 21st century (2071-2100) the differences between regions and scenarios and between RCMs and AOGCMs are apparent (Fig. 4.12). In winter, the temperature increase ranges mostly between 4 and 6°C in the north and between 3 and 5°C in the south. If all projections are taken into account, the interval is greater, and a handful AOGCMs project temperature increases of around 8°C in the northern region. As commonly reported (*e.g.* Christensen *et al.*, 2007, Kjellström *et al.*, 2005, Persson *et al.*, 2007) the winter precipitation in these latitudes is projected to increase and relatively more so as ones moves further north. In Sweden, the AOGCMs project around 10-40% more precipitation, more weighted towards higher values in the north and in stronger forcing scenarios. Considering the RCMs, the A2 runs with ECHAM4 and CCSM3 as forcing AOGCM shows the among the largest increases in both temperature and precipitation. But, also other simulations with A1B emissions show strong response in some seasons for parts of Sweden (*e.g.* HadCM3(high and low) in winter). The strong increase in the downscaling of ECHAM4 is partly related to the fact that the ECHAM4 model projected a strong climate change signal in both temperature and precipitation. But, there is also a contribution to the strong increase in precipitation from the RCA3 model. Kjellström and Lind (2009) have shown that the regional model shows a stronger change in the hydrological cycle in the area than does the corresponding AOGCM, at least in the case of ECHAM5.

Summer is the season with by far the largest spread among the AOGCMs and among the RCMs (which now for the 2071-2100 time period also include four runs with the coupled RCAO model). The large uncertainty is mostly related to precipitation varying in the south between +/- 30%. Also the temperature change in this region in summer is characterized by a quite considerable interval. The smallest increase in the AOGCMs (seen in a B1 scenario) is around 1°C and the largest more than 5°C (A2 scenario). In northern Sweden, on the other hand, the response in summer is more coherent in all models. For example, almost all AOGCMs and RCMs project an increase in precipitation, although quite moderate; around 5-15%, and thus not entirely above the observed decadal variability of the 20th century. On the outer edges of the interval, one model projects an increase of more than 30% and another projects a decrease of some 15-20%. The temperature increases vary between 1.5 and 6°C in the north and between 1 and 5°C in the south.

The inclusion of pattern-scaled data adds some further information to the projections. Scatter diagrams for the climate change signal relative to 1961-1990 at the three subsequent time slices; 2011-2040, 2041-2070 and 2071-2100 are shown in Figs. 4.13-4.14. The pattern of the signal in all the scaled scenarios are the same (given by a_T in Eq. 2), however the amplitude varies, being higher for the A1FI than for the A1T and B2 scenarios. The latter two shows similar responses, although A1T data have slightly larger temperature and precipitation increases. Also, compared to B1, these two scenarios put more weight towards higher precipitation rates in northern summer and towards lower precipitation rates in southern summer.

In winter, the trend is clear; the stronger the scenario the wetter and warmer are the projections. Consequently, the B2 and A1T projections more or less fill up the gap between B1 and A1B. In both seasons and regions A1FI weighs heavily towards warmer temperatures. This is evident in winter, where a few AOGCMs show temperature increases of nearly 12°C in the north and 8-9°C in the south. The precipitation increase is also significantly larger in these AIFI projections, reaching nearly 50% in the south and around 60% in the northern region, i.e. close to the A2-runs with boundaries from ECHAM4 and CCSM3,.

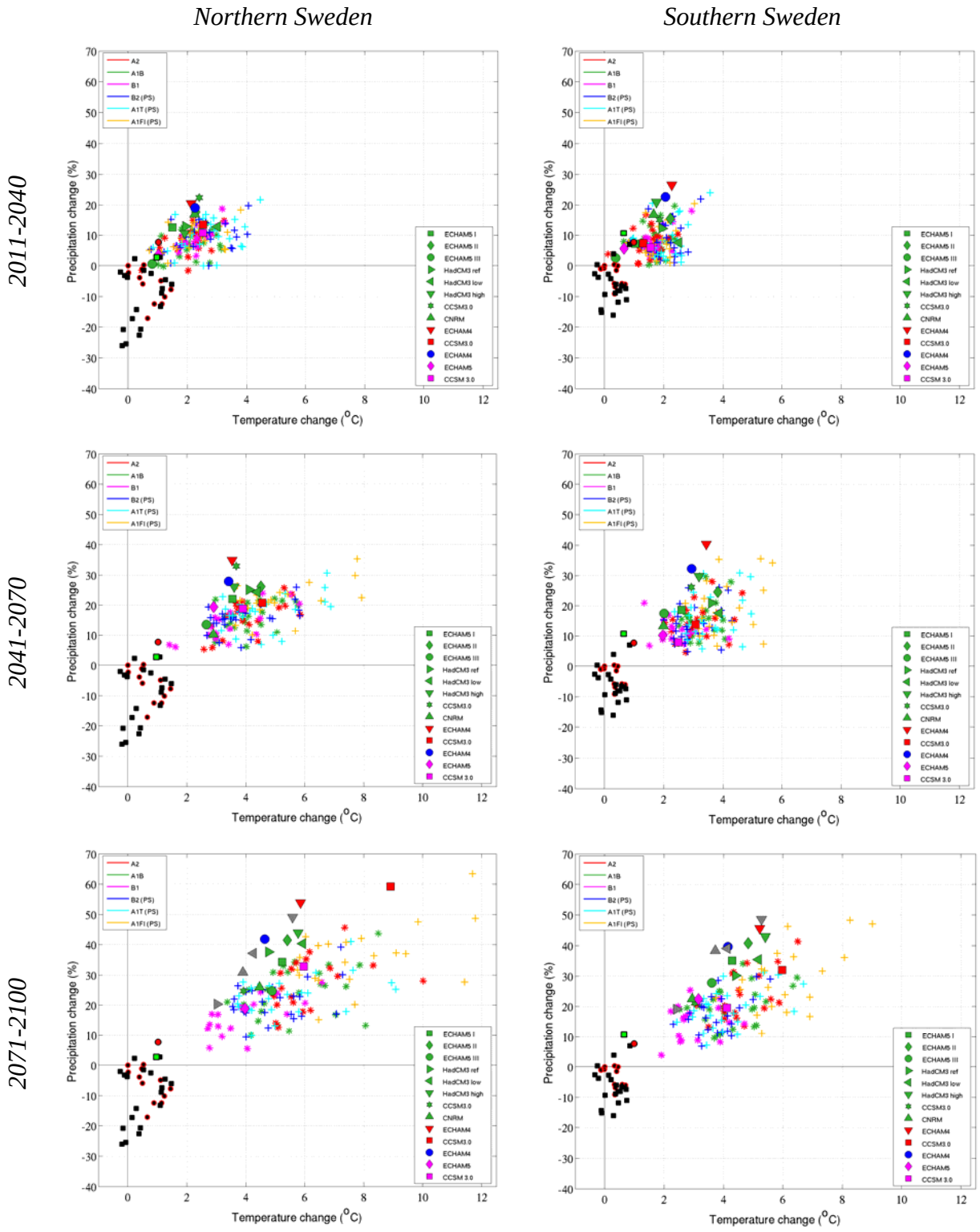

Figure 4.13. *Scatter diagram showing simulated 2m-temperature and precipitation changes compared to 1961-1990 for three subsequent 30-year periods in winter (DJF) in northern (left) and southern (right) Sweden. Included is also pattern-scaled (PS) data ('plus' markers), increasing the number of scenarios to represent all the six marker scenarios. The black squares and circles represent the SMHI and CRU observations respectively. The filled green square and red circle are the latest observed tri-decadal mean. The stars (*) denote the GCMs with colouring according to the left upper legend. The same colour scale applies to the right legend showing the RCA3 experiments with labels according to forcing GCM.*

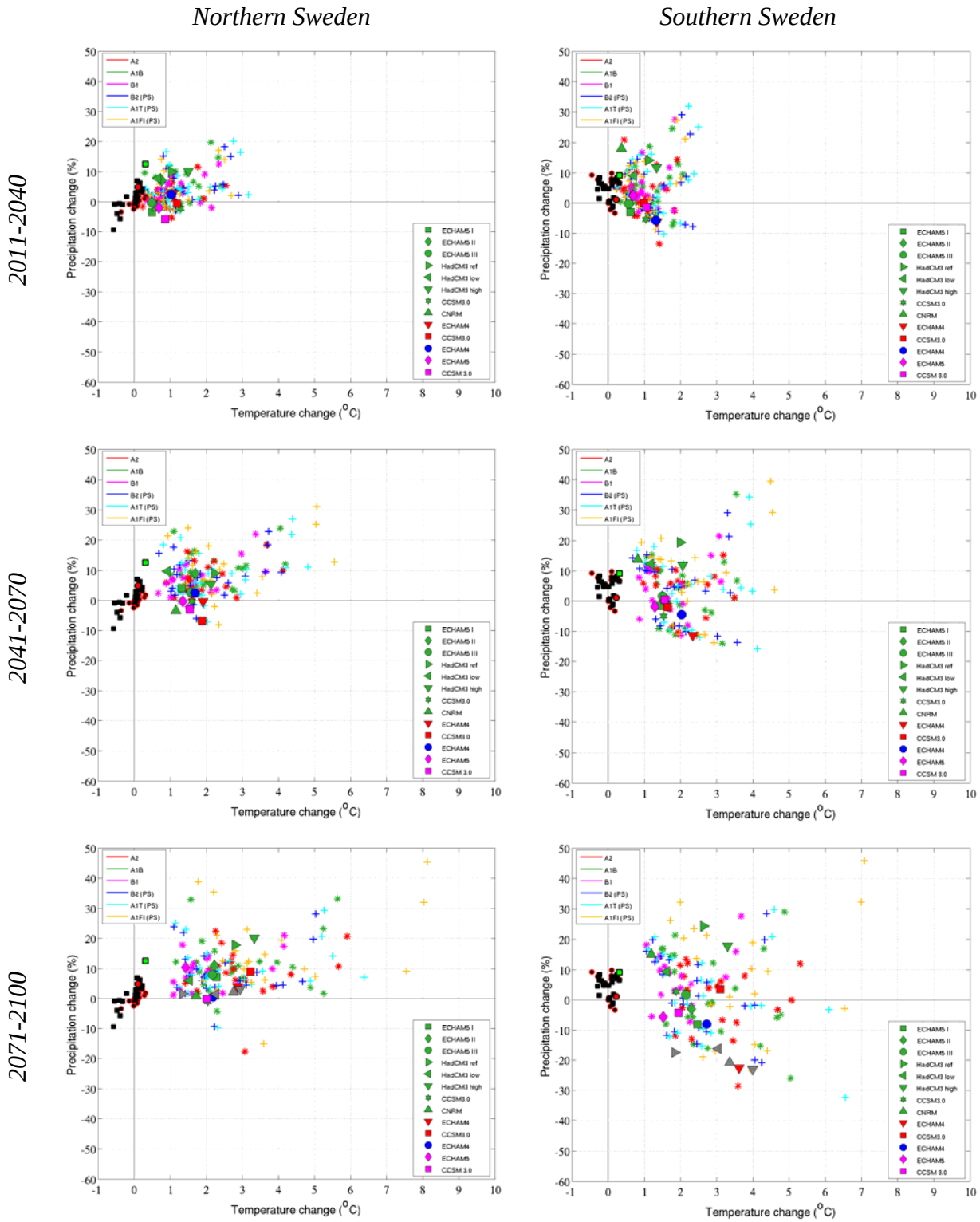

Figure 4.14. *Scatter diagram showing simulated 2m-temperature and precipitation changes compared to 1961-1990 for three subsequent 30-year periods in summer (JJA) in northern (left) and southern (right) Sweden. Included is also pattern-scaled (PS) data ('plus' markers), increasing the number of scenarios to represent all the six marker scenarios. The black squares and circles represent the SMHI and CRU observations respectively. The filled green square and red circle are the latest observed tri-decadal mean. The stars (*) denote the GCMs with colouring according to the left upper legend. The same colour scale applies to the right legend showing the RCA3 experiments with labels according to forcing GCM.*

To provide further details of, and to summarize, the AOGCM results averaged over all six emission scenarios, Table 4.1 shows general statistics of the simulated and pattern-scaled data. During winter, the mean temperature increase in the period 2071-2100 is 5.7°C in the north and 4.4°C in the south, whereas in summer it is lower; 2.9°C and 2.8°C respectively. The median temperature increase is not more than 0.5°C from the mean increase in both seasons and regions. Furthermore, the upper and lower quartiles reveal that 50% of the simulations constrain the winter (summer) temperature changes to 4.2-6.7°C (1.9-3.6°C) and 3.4-5.1°C (1.8-3.7°C) in northern and southern Sweden respectively.

Another statistical estimate, the 95% confidence interval, can be calculated assuming that the changes depict a normal distribution. Ruosteenoja *et al.* (2007) produced quantile-plots and validated simulated values with corresponding values in a normal distribution. They found a good agreement for temperature and precipitation in a group of regions in Europe (including northern Europe). Assuming normal distribution also in the present data sets we calculate the 95% confidence interval as presented in Table 4.1. The results depict a wide winter temperature change interval in both parts of Sweden; 2.1-9.3°C and 1.8-6.9°C respectively. In summer the corresponding intervals are; 0.0-5.7°C and 0.3-5.4°C. No decrease in temperature is, thus, present in these wide intervals, although zero changes are included in summer.

The precipitation also follows the seasonal pattern described above; larger increases in winter and most so in the north. In summer the spread is larger including also uncertainty in sign, especially in the south. For example, in summer in southern Sweden, a quarter of the simulations show a decrease of more than 6% while another quarter shows an increase of more than 13%.

Table 4.1. *Statistical estimates of the winter (DJF) and summer (JJA) simulated climate change information for Sweden, calculated for the time period 2071-2100, for all AOGCMs (ensemble averages when available) and scenarios including the pattern-scaled; in total six scenarios and 20 models. The data from the individual models is plotted in the multi-scenario scatter-plots in Figs. 4.13-4.14. The statistical properties include the mean, median, and lower and higher quartile (Q75 and Q25 respectively), as well as the 95% confidence interval (CI95), assuming a normal distribution. See text for details.*

	Northern Sweden		**Southern Sweden**	
	Temp. (°C)	Precip. (%)	Temp. (°C)	Precip. (%)
Winter				
Mean	5.7	25	4.4	21
Median	5.5	24	4.1	20
Q75	6.7	31	5.1	25
Q25	4.2	18	3.4	15
CI95	2.1 – 9.3	6 – 44	1.8 – 6.9	4 – 38
Summer				
Mean	2.9	11	2.8	3
Median	2.4	9	2.5	3
Q75	3.6	14	3.7	13
Q25	1.9	5	1.8	-6
CI95	0.0 – 5.7	-8 – 29	0.3 – 5.4	-24 – 32

In addition to the multi-scenario analysis, results for the respective emission scenarios are quantified in Table 4.2, where the mean values across all AOGCMs and the 95% confidence interval are presented.

Table 4.2. *Statistical estimates of the winter (DJF) and summer (JJA) simulated climate change information for Sweden, calculated for the time period 2071-2100, for all AOGCMs (ensemble values where available) and presented for the respective scenario including the pattern-scaled. The statistical properties include the mean (the middle column) and the 95% confidence interval (CI95; the left column represents the lower limit and the right column the higher limit).*

	Northern Sweden				**Southern Sweden**			
	Temp. (°C)			Precip. (%)	Temp. (°C)			Precip. (%)
Winter								
A1FI	4.3	8.0	11.7	15 35 55	3.6	6.1	8.6	9 29 49
A2	3.7	6.2	8.8	11 27 43	3.2	4.8	6.4	9 24 39
A1T	2.8	5.2	7.6	10 23 36	2.4	4.0	5.6	6 19 32
A1B	2.9	5.6	8.4	8 25 42	2.8	4.3	6.3	7 20 33
B2	2.6	4.9	7.2	9 22 34	2.2	3.8	5.3	5 18 30
B1	1.8	4.1	6.3	6 17 28	1.6	3.1	4.6	3 16 29
Summer								
A1FI	0.2	4.0	7.8	-11 15 41	0.7	3.9	7.2	-35 5 45
A2	0.6	3.1	5.6	-9 8 25	0.9	3.2	5.4	-26 -2 23
A1T	0.1	2.6	5.0	-7 10 27	0.4	2.6	4.7	-22 3 29
A1B	0.4	2.9	5.3	-6 11 29	0.7	2.8	5.0	-22 3 28
B2	0.1	2.5	4.8	-7 9 25	0.4	2.4	4.4	-21 3 28
B1	0.2	2.2	4.1	-3 9 21	0.5	2.1	3.7	-10 7 24

4.2.3 Expanding the matrix by PCA; a statistical approach

As discussed in the introductory section; with the increase in computer resources with time, climatological assessments will be directed towards a more probabilistic approach. This is because a greater number of simulations are enabled, as well as longer integrations and with more climate models, even though there is always a balance between increasing the complexity of the models (for example by including more processes) or increasing the resolution and thereby the amount of data. Availability of ensembles consisting of large numbers of members makes statistical analyses more easily achieved and climate information may be validated and interpreted in a broader sense.

Figs. 4.15 depict the resampled ensemble (See section 3.4) for temperature and precipitation in winter for northern and southern Sweden. Shown are also the extremes in the raw data, corresponding to the values above and below the 95th and 5th percentiles respectively. In both regions, a clear trend in temperature is seen, stronger in the north. This evolution is also seen for precipitation; however, the trends are much weaker. Important to note, though, is that for both variables and regions the contours comprise both negative and positive values, even at the end of the century and for temperature in northern Sweden. This implies that even in scenarios with a strong climate change signal individual years and seasons may be colder than the climatological average in today's climate. The chance thereof is considerably smaller than

in the control period. Negative numbers are most prominent for precipitation, reflecting the large internal variability. Furthermore, the original data (as well as contours for precipitation) show greater spread as time evolves, clearly seen for temperature where the number of blue circles above the outermost contour increases towards the end of the century while those below the 5th percentile remain just about the same. Characteristic for precipitation is that high extremes are almost exclusively concentrated above the outermost contour, in contrast to the low extremes.

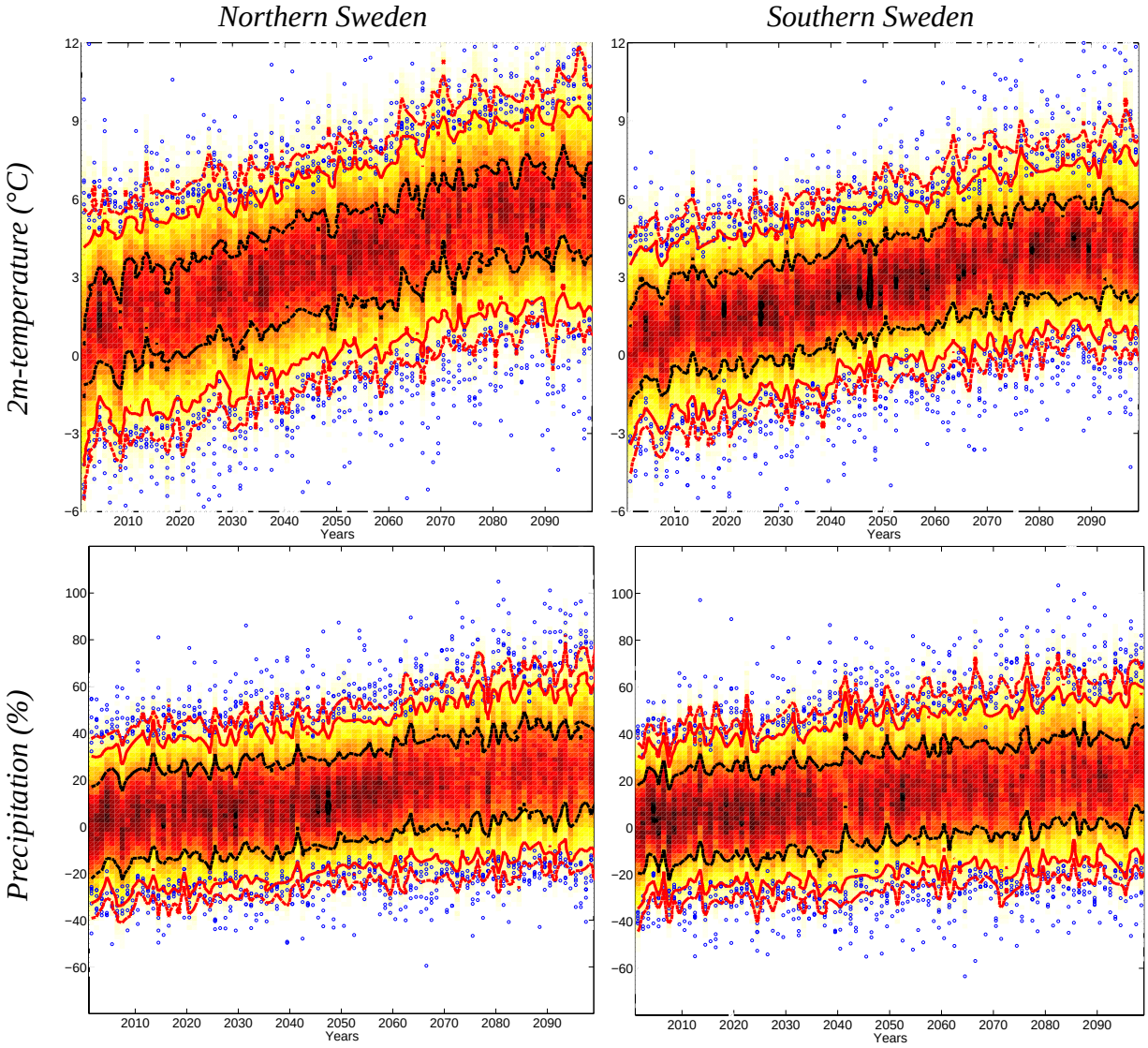

Figure 4.15. *Resampled 2m-temperature (top) and precipitation (bottom) changes in winter (DJF). The original and component-resampled data represent the changes in the 21st century in northern (left) and southern (right) Sweden. 99% of the data are between the dashed red lines, 98% between the full red lines, 95% between the dashed black lines and 90% between the full black lines. Blue circles represent the raw data that are located respectively above and below the 95th and 5th percentiles in the original data set.*

The corresponding resampled ensemble climate evolution in summer is depicted in Figs. 4.16. Typically, the uncertainty increases with time as showed by the presence and absence of the highest value contour in the beginning and the end respectively. Temperature changes indicate long tails of high values by the end of the century as represented by the outermost contour. Raw data extremes (above 95th percentile and below 5th percentile values) are almost entirely

above the high end contour and above the low end for temperature in both regions, not seen in winter. The larger uncertainty towards the end reflects both the divergence between models and larger differences in emission scenarios at that time.

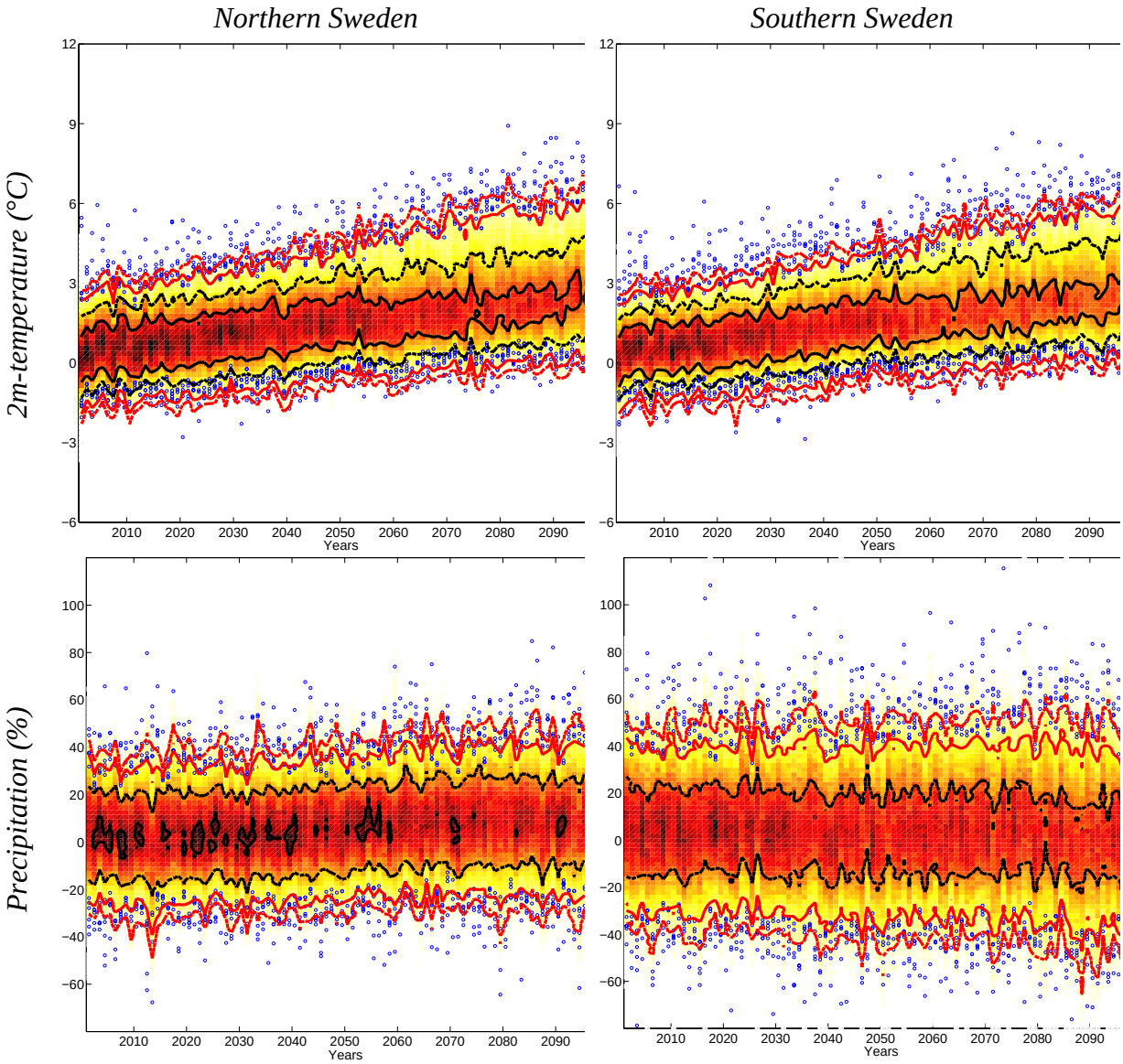

Figure 4.16. *Resampled 2m-temperature (top) and precipitation (bottom) changes in summer (JJA). The original and component-resampled data represent the changes in the 21st century in northern (left) and southern (right) Sweden. 99% of the data are between the dashed red lines, 98% between the full red lines, 95% between the dashed black lines and 90% between the full black lines. Blue circles represent the raw data that are located respectively above and below the 95th and 5th percentiles in the original data set.*

To condense the resampled ensemble data into a more comprehensible form, statistical estimates (same as in Table 4.1) are calculated and assembled in Table 4.3. The results shows that even though the mean remains about the same as in Table 4.1, the quartiles and the 95% confidence interval are different, expanding the intervals of uncertainty. For example, 50% of the data represents the interval 3.9 – 7.2°C (4.2 – 6.7°C in Table 4.1) for winter temperature in the north, and the corresponding 95% confidence interval increases to 0.6 – 10.5°C, and thus, temperature changes close to 0°C are present. Considering precipitation, the ensemble display quite significant uncertainties; in northern winter the confidence interval is -20 – 69%,

i.e. both signs of change are present. In southern Sweden the uncertainty is even larger, as expected, with an interval of -48 – 54% (-24 – 32% in Table 4.1). Here, a quarter of the data have decreases in precipitation greater than 14% and an equal amount have increases above 20% (corresponding interval is -6% – 13% in Table 4.1).

Table 4.3. *Statistical properties of the simulated climate information, after the data has been post-processed in a PCA analysis and then recombined into a larger ensemble (see text). The data is based on the 2071-2099 time period from all AOGCMs (ensemble averages when available) and scenarios including the pattern-scaled; in total six scenarios and 20 models. The statistical properties include the mean, median, and lower and higher quartile (Q75 and Q25 respectively), as well as the 95% confidence interval (CI95), assuming a normal distribution.*

	Northern Sweden		**Southern Sweden**	
	Temp. (°C)	Precip. (%)	Temp. (°C)	Precip. (%)
Winter				
Mean	5.6	24	4.2	22
Median	5.5	24	4.2	21
Q75	7.2	39	5.5	36
Q25	3.9	9	2.9	7
CI95	0.6 – 10.5	-20 – 69	0.2 – 8.3	-22 – 65
Summer				
Mean	2.7	9	2.7	3
Median	2.6	9	2.6	3
Q75	3.7	22	3.7	20
Q25	1.7	-3	1.7	-14
CI95	-0.3 – 5.8	-28 – 47	-0.1 – 5.6	-48 – 54

5. Summary and Conclusions

In this report, we perform an analysis of climate change projections for northern and southern Sweden as simulated in more than twenty AOGCMs used in the IPCCs fourth assessment report (IPCC, 2007). We compare these results to results from regional climate model simulations with the Rossby Centre regional climate model. To provide a comprehensive analysis, as much data as possible should be included. Furthermore, a greater amount of data justifies a statistical approach that may give an enhanced appreciation of the climate changes. Accordingly, a pattern-scaling method was used to increase the number of scenarios with the AOGCMs, and, additionally, a decomposition-recombination method was applied to further increase the ensemble size. The main results of the study are:

- Seasonal cycles in surface temperature in the control period (1961-1990) shows some deviations compared to reanalysis data and observations, represented by ERA40 and CRU TS 2.1 gridded data respectively. A general cold bias in winter is evident in most AOGCMs particularly in northern Sweden. Most models are too cold also during summer. The temperature biases amount to 2-5°C for single months in the multi-model ensemble mean and occasionally up to 10°C in single models. This cold bias is consistent with a too weak north-southerly pressure gradient over Europe as compared to ERA40. Such a weak

pressure gradient is indicative of weaker than observed westerly winds on average which implies that the climate is too heavily influenced by cold continental air masses.

- The precipitation climate shows larger relative discrepancies to observations compared to the temperature climate, which is expected due to the dependence on resolution that is often too coarse in the AOGCMs to accurately capture meso-scale phenomena such as orographically forced precipitation production and extreme values. By and large the AOGCMs have too much precipitation in all seasons except summer where the tendencies are opposite. Biases differ significantly between the models and ranges from around +/- 50% in northern Sweden and reaching over 100% in some models in southern Sweden during the cold season.

- After adjustment of mean biases we have shown that the internal variability for the 1961-1990 period in the respective AOGCMs represented by different ensemble members is very similar to the observed variability of the 20th century as given by partly overlapping tri-decal means from two different data sets. Bearing in mind that the number of ensemble members with each AOGCM is restricted and that the observed 20th century climate shows long-term change this good agreement lends confidence to the ability of the AOGCMs to sample the decadal variability at the seasonal scale in the north European area.

- The projections of future temperature and precipitation changes are presented in scatter-diagrams. Compared to the natural variability, represented by observations from the late 19th and the whole 20th century, changes in both northern and southern Sweden is evident already in the near future (2011-2040), most obvious for wintertime temperature. In southern Sweden the spread in summer precipitation is large and cannot be separated from natural variability. When moving forward into the 21st century, the climate change signal gradually becomes stronger and stronger. Furthermore, the signal is dependent on the radiative forcing; the high emission scenarios project larger temperature increases in all seasons and greater increases (decreases) in winter (summer) precipitation. By the end of the 21st century, the mean simulated (including pattern-scaled) increase over all scenarios in winter (summer) temperature ranges from 5.8°C (2.9) and 4.5°C (2.8) in northern and southern Sweden respectively. The corresponding values for precipitation are +25% (+21) and +11% (+4).

- To further increase the amount data of future climate states, a mathematical approach is applied, where the signals from all the available runs including different scenarios are decomposed by a principal component analysis. The obtained coefficients for the orthogonal eigenvectors are then recombined a large number of times, thereby increasing the ensemble size significantly. The results were collected in a number of statistical measures, and they presented a broadening of the uncertainty intervals by the end of the century compared to the simulated data; the middle 50% of the members in the enlarged ensemble showed an increase in winter temperature between 3.9 and 7.2°C in northern Sweden, and between 2.9 and 5.5°C in the southern part. Also, the spread in precipitation change is considerable; for example the summer values in southern Sweden ranges between -14% and +20%.

- Results partitioned on emission scenario show a considerable impact of emissions by the end of the century in this area. Seasonal mean winter (DJF) temperature in northern Sweden is projected to increase by 4.1°C in the B1 and by 8.0°C in the A1FI scenarios

respectively. Corresponding numbers are 2.2°C and 4.0°C in summer. The response in southern Sweden is very similar to that in the north in summer while wintertime increases are 1-2°C weaker than in the north. Confidence intervals calculated for all emission scenarios reveals very broad ranges of future temperature increases. 95% confidence intervals reveal a total range over all scenarios between 1.8-11.7°C in the north and 1.6-8.6°C in the south for winter.

- The regional climate signals, as projected by the RCA3 and RCAO models, are in large part within the limits of the AOGCM runs. Considering temperature, they are more or less located near the major group of the AOGCMs, although the spread between the individual projections is evident. In terms of precipitation there is a tendency for the RCM simulations to show a stronger climate change signal than the AOGCMs in winter while they are more in the range of the AOGCMs in summer.

- Also in the regional climate change simulations the differences between different emission scenarios becomes more evident with time with stronger response the stronger the forcing is. But, this relation does not hold everywhere for all seasons and variables as the RCM simulations show a considerable spread also at the end of the 21st century. Clearly, a major source of uncertainty is the choice of AOGCM providing boundary conditions. In earlier time periods of the 21st century the results also show a strong impact of the natural variability as simulated by the AOGCMs. This has been demonstrated by the three A1B runs with RCA3 downscaling ECHAM5

One must bear in mind, though, that this report provides no detailed evaluation of the regional signals in the AOGCMs and RCMs, as it would require a deeper analysis of a greater number of variables and on more spatio-temporal scales, as well as a more detailed examination of the model physics and structure. Therefore, the results presented here should more be emphasized as guidelines for users that wish to have some general appreciation of the climate change projections for Sweden, as simulated by AOGCMs and RCMs. Furthermore, it should be noted that the derived uncertainty ranges are conditional to the specific scenarios that we have analysed. A larger number of emission scenarios or a larger number of ensemble members may change the uncertainty ranges. Also, even with an infinite number of scenarios with the available models we can not be certain to capture the full uncertainty range as such an ensemble would be conditional on the model formulation of the AOGCMs that we use.

Acknowledgements

This work is part of the Mistra-SWECIA programme, funded by Mistra (the Foundation for Strategic Environmental Research), and of the ENSEMBLES project funded by the EC through contract GOCE-CT-2003-505539. Many of the model simulations with the regional climate model were performed on the climate computing resource Tornado funded with a grant from the Knut and Alice Wallenberg foundation. The ECHAM4/OPYC3 and ECHAM5/MPI-OM1 global simulations were kindly provided by the Max Planck Institute for Meteorology in Hamburg, Germany, and the Danish Meteorological Institute in Copenhagen. The HadCM3 global simulations were provided by the Hadley Centre, Exeter, United Kingdom. Further we acknowledge the modelling groups, the Program for Climate Model Diagnosis and Intercomparison (PCMDI) and the WCRP's Working Group on Coupled Modelling (WGCM) for their roles in making available the WCRP CMIP3 multi-model dataset. Support of this dataset is provided by the Office of Science, U.S. Department of Energy. We are grateful to Dr Sarah Raper and Dr Kimmo Ruosteenoja for supplying the MAGICC data.

References

Alexandersson, H., 2002. Temperatur och nederbörd I Sverige 1860-2001. *Rapport i Meteorologi,* 104, SMHI, SE 601 76 Norrköping, Sweden 28 pp.

Alexandersson H, Moberg A., 1997. Homogenization of Swedish temperature data. Part I: Homogeneity test for linear trends. *Int. J. Climatol*. **17**, 25-34.

Christensen, J.H., B. Hewitson, A. Busuioc, A. Chen, X. Gao, I. Held, R. Jones, R.K. Kolli, W.-T. Kwon, R. Laprise, V. Magaña Rueda, L. Mearns, C.G. Menéndez, J. Räisänen, A. Rinke, A. Sarr and P. Whetton, 2007: Regional Climate Projections. In: *Climate Change 2007: The Physical Science Basis. Contribution of Working Group I to the Fourth Assessment Report of the Intergovernmental Panel on Climate Change* [Solomon, S., D. Qin, M. Manning, Z. Chen, M. Marquis, K.B. Averyt, M. Tignor and H.L. Miller (eds.)]. Cambridge University Press, Cambridge, United Kingdom and New York, NY, USA.

Christensen, J.H. and Christensen, O.B., 2007, A summary of the PRUDENCE model projections of changes in European climate by the end of this century. *Climatic Change*, **81**:7-30. doi: 10.1007/s10584-006-9210-7

Collins, M., Booth, B.B.B., Harris, G.R., Murphy, J.M., Sexton, D.M.H. and Webb, M.J., 2006: Towards quantifying uncertainty in transient climate change. *Climate Dynamics*, **27**, 127-147. doi:10.1007/s00382-006-0121-0.

Cubasch, U., Meehl, G.A., Boer, G.J., Stouffer, R.J., Dix, M., Noda, A., Senior, C.A., Raper, S. and Yap, K.S., 2001. Projections of future climate change. In: Climate Change 2001: The Scientific Basis. Contribution of Working Group I to the Third Assessment Report of the Intergovernmental Panel on Climate Change. Houghton, J.T., Ding, Y., Griggs, D.J., Noguer, M., van der Linden, P.J., Dai, K., Maskell, K. and Johnson, C.A. (eds). Cambridge University Press, Cambridge, U.K., 881 pp.

Déqué, M., Rowell, D.P., Lüthi, D., Giorgi, F., Christensen, J.H., Rockel, B., Jacob, D., Kjellström, E., de Castro, M. and van den Hurk, B., 2007: An intercomparison of regional climate simulations for Europe: assessing uncertainties in model projections. *Climatic Change*. **81**, 53-70. doi:10.1007/s10584-006-9228-x.

Dettinger, M., 2006. A component-resampling approach for estimating probability distributions from small forecast ensembles. *Climatic Change*,. DOI: 10.1007/s10584-005-9001-6.

Döscher, R., Willén, U., Jones, C., Rutgersson, A., Meier, H. E. M., Hansson, U. and Graham, L.P., 2002. The development of the coupled regional ocean-atmosphere model RCAO. *Boreal Environment Research* **7***,* 183-192.

Giorgi, F., Hewitson, B., Christensen, J., Hulme, M., Von Storch, H., Whetton, P., Jones, R., Mearns, L. and Fu, C., 2001. Regional Climate Information – Evaluation and Projections. In: *Climate Change 2001: The Scientific Basis. Contribution of Working Group I to the Third Assessment Report of the Intergovernmental Panel on Climate Change.* Houghton, J.T., Ding, Y., Griggs, D.J., Noguer, M., van der Linden, P.J., Dai, K., Maskell, K. and Johnson, C.A. (eds). Cambridge University Press, Cambridge, U.K., 881 pp.

Graham, L., P., Chen, D., Christensen, O.B., Kjellström, E., Krysanova, V., Meier, H.E.M., Radziejewski, M., Rockel, B., Ruosteenoja, K. and Räisänen, J., 2008. Projections of future climate change. In *Assessment of Climate Change for the Baltic Sea Basin.* The BACC Author Team. 2008, XXI, 473 p., ISBN: 978-3-540-72785-9.

Hewitt, C.D and Griggs, D.J., 2004: Ensembles-based predictions of climate changes and their impacts. *Eos*, **85**, 566.

Hurrell, J.W., 1995. Decadal trends in North Atlantic Oscillation: Regional temperatures and precipitation. *Science*, **269**, 676-679.

IPCC, 2001. *Climate Change 2001: The Scientific Basis. Contribution from Working Group I to the Third Assessment Report of the Intergovernmental Panel on Climate Change* [Houghton, J.T., Y.Ding, D.J. Griggs, M. Noguer, P.J. van der Linden, X. Dai, K. Maskell, and C.A. Johnson (eds.)]. Cambridge University Press, Cambridge, United Kingdom and New York, NY, USA, 881 pp.

IPCC, 2007: Climate Change 2007: The Physical Science Basis. Contribution of Working Group I to the Fourth Assessment Report of the Intergovernmental Panel on Climate Change [Solomon, S., D. Qin, M. Manning, Z. Chen, M. Marquis, K.B. Averyt, M. Tignor and H.L. Miller (eds.)]. Cambridge University Press, Cambridge, United Kingdom and New York, NY, USA, 996 pp.

Jones, C.G., Ullerstig, A., Willén, U. and Hansson, U., 2004. The Rossby Centre regional atmospheric climate model (RCA). Part I: Model climatology and performance characteristics for present climate over Europe. *Ambio*, **33**(4-5), 199-210.

Kalnay E., Kanamitsu M., Kistler R., Collins W., Deaven D., Gandin L., Iredell M., Saha S., White G., Woollen J., Zhu Y., Chelliah M., Ebisuzaki W., Higgins W., Janowiak J., Mo K.C., Ropelewski C., Wang J., Leetmaa A., Reynolds R., Jenne R. and Joseph D., 1996. The NCEP/NCAR 40-Year Reanalysis Project, *Bull. Amer. Met. Soc.* 77:437--471.

Källén, E., 1996. HIRLAM Documentation Manual 2.5. *Technical Report.*, SMHI, SE 601 76 Norrköping, Sweden.

Kjellström, E., Bärring, L., Gollvik, S., Hansson, U., Jones, C., Samuelsson, P., Rummukainen, M., Ullerstig, A., Willén U. and Wyser, K., 2005. A 140-year simulation of European climate with the new version of the Rossby Centre regional atmospheric climate model (RCA3). *Reports Meteorology and Climatology*, 108, SMHI, SE-60176 Norrköping, Sweden, 54 pp.

Kjellström, E. and Ruosteenoja, K., 2007. Present-day and future precipitation in the Baltic Sea region as simulated in a suite of regional climate models. *Climatic Change*. **81**, 281-291.

Kjellström, E. and Lind, P., 2009. Changes in the water budget in the Baltic Sea drainage basin in future warmer climates as simulated by the regional climate model RCA3. *Boreal Env. Res*. **14**, 114–124.

Kjellström, E., Brandefelt, J., Näslund, J.O., Smith, B., Strandberg, G. and Wohlfarth, B, 2009: Climate conditions in Sweden in a 100,000 year time perspective. Svensk Kärnbränslehantering AB, report TR-09-04, 133 pp.

Lind, P. and Kjellström, E., 2009. Water budget in the Baltic Sea drainage basin: Evaluation of simulated fluxes in a regional climate model. *Boreal Env. Res.* **14**, 56–67.

Ljungemyr, P., Gustafsson, N and Omstedt, A., 1996. Parameterization of lake thermodynamics in a high resolution weather forecasting model. *Tellus*. **48**A, 608-621.

Lüthi, D., Le Floch, M., Bereiter, B., Blunier, T., Barnola, J.-M., Siegenthaler, U., Raynaud, D., Jouzel, J., Fischer, H., Kawamura, K. and Stocker, T.F., 2008. High-resolution carbon dioxide concentration record 650,000–800,000 years before present. *Nature* **453**, 379-382.

Meehl, G.A., T.F. Stocker, W.D. Collins, P. Friedlingstein, A.T. Gaye, J.M. Gregory, A. Kitoh, R. Knutti, J.M. Murphy, A. Noda, S.C.B. Raper,I.G. Watterson, A.J. Weaver and Z.-C. Zhao, 2007: Global Climate Projections. In: *Climate Change 2007: The Physical Science Basis. Contribution of Working Group I to the Fourth Assessment Report of the Intergovernmental Panel on Climate Change* [Solomon, S.,D. Qin, M. Manning, Z. Chen, M. Marquis, K.B. Averyt, M. Tignor and H.L. Miller (eds.)]. Cambridge University Press, Cambridge, United Kingdom and New York, NY, USA.

Meier, H.E.M., Döscher, R. Coward, A., Nycander, J. and Döös, K., 1999. RCO – Rossby Centre regional ocean climate model: model description (version 1.0) and first results from the hindcast period 1992/1993. *Reports Oceanography* 26, SMHI, SE 60176 Norrköping, Sweden, 102 pp.

Meier, H.E.M., Döscher, R. and Faxén, T., 2003. A multiprocessor coupled ice-ocean model for the Baltic Sea. Application to the salt inflow. *J. Geophys. Res.* **108**, C8, 3273.

Mitchell, T.D., 2003. Pattern Scaling: An Examination of the Accuracy of the Technique for Describing Future Climates. *Climatic Change*, **60**(3), 217-242.

Mitchell T.D. & Jones P.D., 2005. An improved method of constructing a database of monthly climate observations and associated high-resolution grids. Int. J. Climatol. 25: 69-712.

Murphy, J. M., Booth, B. B. B., Collins, M., Harris, G. R., Sexton, D. and Webb, M., 2007. A methodology for probabilistic predictions of regional climate change from perturbed physics ensembles. *Phil. Trans. R. Soc. A*, **365**, 1993-2028.

Nakićenović, N., Alcamo, J., Davis, G., de Vries, B., Fenhann, J., Gaffin, S., Gregory, K., Grübler, A., *et al*., 2000. Emission scenarios. A Special Report of Working Group III of the Intergovernmental Panel on Climate Change. Cambridge University Press, 599 pp.

Persson, G., Bärring, L., Kjellström, E., Strandberg, G. and Rummukainen, M., 2007. Climate indices for vulnerability assessments. *Reports Meteorology and Climatology*, 111, SMHI, SE-60176 Norrköping, Sweden, 64 pp.

Räisänen, J., Hansson, U., Ullerstig, A., Döscher, R., Graham, L.P., Jones, C., Meier, M., Samuelsson, P. and Willén, U., 2003. GCM driven simulations of recent and future climate with the Rossby Centre coupled atmosphere – Baltic Sea regional climate model RCAO, *Reports Meteorology and Climatology* 101, SMHI, SE 60176 Norrköping, Sweden, 61 pp.

Räisänen, J., U. Hansson, A. Ullerstig, R. Döscher, L.P. Graham, C. Jones, H.E.M. Meier, P. Samuelsson, U. Willén, 2004. European climate in the late 21st century: regional simulations with two driving global models and two forcing scenarios. *Climate Dynamics*, **22**, 13-31.

Randall, D.A., R.A. Wood, S. Bony, R. Colman, T. Fichefet, J. Fyfe, V. Kattsov, A. Pitman, J. Shukla, J. Srinivasan, R.J. Stouffer, A. Sumi and K.E. Taylor, 2007: Climate Models and Their Evaluation. In: Climate Change 2007: The Physical Science Basis. Contribution of Working Group I to the Fourth Assessment Report of the Intergovernmental Panel on Climate Change [Solomon, S., D. Qin, M. Manning, Z.

Chen, M. Marquis, K.B. Averyt, M.Tignor and H.L. Miller (eds.)]. Cambridge University Press, Cambridge, United Kingdom and New York, NY, USA.

Rummukainen, M., Räisänen, J., Bringfelt, B., Ullerstig, A., Omstedt, A., Willén, U., Hansson, U. and Jones, C., 2001. A regional climate model for northern Europe: model description and results from the downscaling of two GCM control simulations. *Climate Dynamics*, **17**, 339-359.

Ruosteenoja, K., Carter, T.R., Jylhä, K. and Tuomenvirta, H., 2003. Future climate in world regions: An intercomparison of model-based projections for the new IPCC emission scenarios. *The Finnish Environment* **644**, Finnish Environment Institute, 83 pp.

Ruosteenoja, K., Tuomenvirta, H. and Jylhä, K., 2007. GCM-based regional temperature and precipitation change estimates for Europe under four SRES scenarios applying a super-ensemble pattern-scaling method. *Climatic Change*, **81** 193-198.

Samuelsson, P., Gollvik, S. and Ullerstig, A., 2006. The land-surface scheme of the Rossby Centre regional atmospheric climate model (RCA3). *SMHI Meteorologi No 122* . 25 pp.

SOU, 2007. Sverige inför klimatförändringarna – hot och möjligheter. Slutbetänkande av Klimat- och sårbarhetsutredningen. Statens offentliga utredningar. SOU 2007:60. Stockholm, Sverige. ISBN 978-91-38-22793-0. (in Swedish).

van Ulden, A.P., and van Oldenborgh, G.J., 2006: Large-scale atmospheric circulation biases and changes in global climate model simulations and their importance for climate change in Central Europe. *Atmos. Chem. Phys*., **6**, 863–881.

Uppala S.M., Kållberg P.W., Simmons A.J., Andrae U., da Costa Bechtold V., Fiorino M., Gibson J.K., Haseler J., Hernandez A., Kelly G.A., Li X., Onogi K., Saarinen S., Sokka N., Allan R.P., Andersson E., Arpe K., Balmaseda M.A., Beljaars A.C.M., van de Berg L., Bidlot J., Bormann N., Caires S., Chevallier F., Dethof A., Dragosavac M., Fisher M., Fuentes M., Hagemann S., Holm E., Hoskins B.J., Isaksen L., Janssen P.A.E.M., Jenne R., McNally A.P., Mahfouf J.-F., Morcrette J.-J., Rayner N.A, Saunders R.W., Simon P., Sterl A., Trenberth K.E., Untch A., Vasiljevic D., Viterbo P. & Woollen J., 2005. The ERA-40 reanalysis. *Q. J. Roy. Meteorol. Soc*. **131**, 2961--3012.

Wigley, T.M.L., 1994. *MAGICC (Model for the Assessment of Greenhouse-gas Induced Climate Change): User's Manual and Scientific Reference Manual.* Boulder, Colo.: National Center for Atmospheric Research.

SMHI Publications

SMHI publishes six report series. Three of these, the R-series, are intended for international readers and are in most cases written in English. For the others the Swedish language is used.

Names of the Series	Published since
RMK (Report Meteorology and Climatology)	1974
RH (Report Hydrology)	1990
RO (Report Oceanography)	1986
METEOROLOGI	1985
HYDROLOGI	1985
OCEANOGRAFI	1985

Earlier issues published in serie RMK

1 Thompson, T., Udin, I. and Omstedt, A. (1974)
Sea surface temperatures in waters surrounding Sweden.

2 Bodin, S. (1974)
Development on an unsteady atmospheric boundary layer model.

3 Moen, L. (1975)
A multi-level quasi-geostrophic model for short range weather predictions.

4 Holmström, I. (1976)
Optimization of atmospheric models.

5 Collins, W.G. (1976)
A parameterization model for calculation of vertical fluxes of momentum due to terrain induced gravity waves.

6 Nyberg, A. (1976)
On transport of sulphur over the North Atlantic.

7 Lundqvist, J.-E. and Udin, I. (1977)
Ice accretion on ships with special emphasis on Baltic conditions.

8 Eriksson, B. (1977)
Den dagliga och årliga variationen av temperatur, fuktighet och vindhastighet vid några orter i Sverige.

9 Holmström, I., and Stokes, J. (1978)
Statistical forecasting of sea level changes in the Baltic.

10 Omstedt, A. and Sahlberg, J. (1978)
Some results from a joint Swedish-Finnish sea ice experiment, March, 1977.

11 Haag, T. (1978)
Byggnadsindustrins väderberoende, seminarieuppsats i företagsekonomi, B-nivå.

12 Eriksson, B. (1978)
Vegetationsperioden i Sverige beräknad från temperaturobservationer.

13 Bodin, S. (1979)
En numerisk prognosmodell för det atmosfäriska gränsskiktet, grundad på den turbulenta energiekvationen.

14 Eriksson, B. (1979)
Temperaturfluktuationer under senaste 100 åren.

15 Udin, I. och Mattisson, I. (1979)
Havsis- och snöinformation ur datorbearbetade satellitdata - en modellstudie.

16 Eriksson, B. (1979)
Statistisk analys av nederbördsdata. Del I. Arealnederbörd.

17 Eriksson, B. (1980)
Statistisk analys av nederbördsdata. Del II. Frekvensanalys av månadsnederbörd.

18 Eriksson, B. (1980)
Årsmedelvärden (1931-60) av nederbörd, avdunstning och avrinning.

19 Omstedt, A. (1980)
A sensitivity analysis of steady, free floating ice.

20 Persson, C. och Omstedt, G. (1980)
En modell för beräkning av luftföroreningars spridning och deposition på mesoskala.

21 Jansson, D. (1980)
Studier av temperaturinversioner och vertikal vindskjuvning vid Sundsvall-Härnösands flygplats.

22 Sahlberg, J. and Törnevik, H. (1980)
A study of large scale cooling in the Bay of Bothnia.

23 Ericson, K. and Hårsmar, P.-O. (1980)
Boundary layer measurements at Klock-rike. Oct. 1977.

24 Bringfelt, B. (1980)
A comparison of forest evapotranspiration determined by some independent methods.

25 Bodin, S. and Fredriksson, U. (1980)
Uncertainty in wind forecasting for wind power networks.

26 Eriksson, B. (1980)
Graddagsstatistik för Sverige.

27 Eriksson, B.(1981)
Statistisk analys av nederbördsdata. Del III. 200-åriga nederbördsserier.

28 Eriksson, B. (1981)
Den "potentiella" evapotranspirationen i Sverige.

29 Pershagen, H. (1981)
Maximisnödjup i Sverige (perioden 1905-70).

30 Lönnqvist, O. (1981)
Nederbördsstatistik med praktiska tillämpningar.
(Precipitation statistics with practical applications.)

31 Melgarejo, J.W. (1981)
Similarity theory and resistance laws for the atmospheric boundary layer.

32 Liljas, E. (1981)
Analys av moln och nederbörd genom automatisk klassning av AVHRR-data.

33 Ericson, K. (1982)
Atmospheric boundary layer field experiment in Sweden 1980, GOTEX II, part I.

34 Schoeffler, P. (1982)
Dissipation, dispersion and stability of numerical schemes for advection and diffusion.

35 Undén, P. (1982)
The Swedish Limited Area Model. Part A. Formulation.

36 Bringfelt, B. (1982)
A forest evapotranspiration model using synoptic data.

37 Omstedt, G. (1982)
Spridning av luftförorening från skorsten i konvektiva gränsskikt.

38 Törnevik, H. (1982)
An aerobiological model for operational forecasts of pollen concentration in the air.

39 Eriksson, B. (1982)
Data rörande Sveriges temperaturklimat.

40 Omstedt, G. (1984)
An operational air pollution model using routine meteorological data.

41 Persson, C. and Funkquist, L. (1984)
Local scale plume model for nitrogen oxides. Model description.

42 Gollvik, S. (1984)
Estimation of orographic precipitation by dynamical interpretation of synoptic model data.

43 Lönnqvist, O. (1984)
Congression - A fast regression technique with a great number of functions of all predictors.

44 Laurin, S. (1984)
Population exposure to SO and NO_x from different sources in Stockholm.

45 Svensson, J. (1985)
Remote sensing of atmospheric tempera-ture profiles by TIROS Operational Vertical Sounder.

46 Eriksson, B. (1986)
Nederbörds- och humiditetsklimat i Sverige under vegetationsperioden.

47 Taesler, R. (1986)
Köldperioden av olika längd och förekomst.

48 Wu Zengmao (1986)
Numerical study of lake-land breeze over Lake Vättern, Sweden.

49 Wu Zengmao (1986)
Numerical analysis of initialization procedure in a two-dimensional lake breeze model.

50 Persson, C. (1986)
Local scale plume model for nitrogen oxides. Verification.

51 Melgarejo, J.W. (1986)
An analytical model of the boundary layer above sloping terrain with an application to observations in Antarctica.

52 Bringfelt, B. (1986)
Test of a forest evapotranspiration model.

53 Josefsson, W. (1986)
Solar ultraviolet radiation in Sweden.

54 Dahlström, B. (1986)
Determination of areal precipitation for the Baltic Sea.

55 Persson, C., Rodhe, H. and De Geer, L.-E. (1986)
The Chernobyl accident - A meteorological analysis of how radionucleides reached Sweden.

56 Persson, C., Robertson, L., Grennfelt, P., Kindbom, K., Lövblad, G. och Svanberg, P.-A. (1987)
Luftföroreningsepisoden över södra Sverige 2 - 4 februari 1987.

57 Omstedt, G. (1988)
An operational air pollution model.

58 Alexandersson, H. and Eriksson, B. (1989)
Climate fluctuations in Sweden 1860 - 1987.

59 Eriksson, B. (1989)
Snödjupsförhållanden i Sverige - Säsongerna 1950/51 - 1979/80.

60 Omstedt, G. and Szegö, J. (1990)
Människors exponering för luftföroreningar.

61 Mueller, L., Robertson, L., Andersson, E. and Gustafsson, N. (1990)
Meso-γ scale objective analysis of near surface temperature, humidity and wind, and its application in air pollution modelling.

62 Andersson, T. and Mattisson, I. (1991)
A field test of thermometer screens.

63 Alexandersson, H., Gollvik, S. and Meuller, L. (1991)
An energy balance model for prediction of surface temperatures.

64 Alexandersson, H. and Dahlström, B. (1992)
Future climate in the Nordic region - survey and synthesis for the next century.

65 Persson, C., Langner, J. and Robertson, L. (1994)
Regional spridningsmodell för Göteborgs och Bohus, Hallands och Älvsborgs län. (A mesoscale air pollution dispersion model for the Swedish west-coast region. In Swedish with captions also in English.)

66 Karlsson, K.-G. (1994)
Satellite-estimated cloudiness from NOAA AVHRR data in the Nordic area during 1993.

67 Karlsson, K-G. (1996)
Cloud classifications with the SCANDIA model.

68 Persson, C. and Ullerstig, A. (1996)
Model calculations of dispersion of lindane over Europe. Pilot study with comparisons to easurements around the Baltic Sea and the Kattegat.

69 Langner, J., Persson, C., Robertson, L. and Ullerstig, A. (1996)
Air pollution Assessment Study Using the MATCH Modelling System. Application to sulfur and nitrogen compounds over Sweden 1994.

70 Robertson, L., Langner, J. and Engardt, M. (1996)
MATCH - Meso-scale Atmosperic Transport and Chemistry modelling system.

71 Josefsson, W. (1996)
Five years of solar UV-radiation monitoring in Sweden.

72 Persson, C., Ullerstig, A., Robertson, L., Kindbom, K. and Sjöberg, K. (1996)
The Swedish Precipitation Chemistry Network. Studies in network design using the MATCH modelling system and statistical methods.

73 Robertson, L. (1996)
Modelling of anthropogenic sulfur deposition to the African and South American continents.

74 Josefsson, W. (1996)
Solar UV-radiation monitoring 1996.

75 Häggmark, L. Ivarsson, K.-I. and Olofsson, P.-O. (1997)
MESAN - Mesoskalig analys.

76 Bringfelt, B., Backström, H., Kindell, S., Omstedt, G., Persson, C. and Ullerstig, A. (1997)
Calculations of PM-10 concentrations in Swedish cities- Modelling of inhalable particles

77 Gollvik, S. (1997)
The Teleflood project, estimation of precipitation over drainage basins.

78 Persson, C. and Ullerstig, A. (1997)
Regional luftmiljöanalys för Västmanlands län baserad på MATCH modell-beräkningar och mätdata - Analys av 1994 års data

79 Josefsson, W. and Karlsson, J.-E. (1997)
Measurements of total ozone 1994-1996.

80 Rummukainen, M. (1997)
Methods for statistical downscaling of GCM simulations.

81 Persson, T. (1997)
Solar irradiance modelling using satellite retrieved cloudiness - A pilot study

82 Langner, J., Bergström, R. and Pleijel, K. (1998)
European scale modelling of sulfur, oxidized nitrogen and photochemical oxidants. Model development and evaluation for the 1994 growing season.

83 Rummukainen, M., Räisänen, J., Ullerstig, A., Bringfelt, B., Hansson, U., Graham, P. and Willén, U. (1998)
RCA - Rossby Centre regional Atmospheric climate model: model description and results from the first multi-year simulation.

84 Räisänen, J. and Döscher, R. (1998)
Simulation of present-day climate in Northen Europé in the HadCM2 OAGCM.

85 Räisänen, J., Rummukainen, M., Ullerstig, A., Bringfelt, B., Hansson, U. and Willén, U. (1999)
The First Rossby Centre Regional Climate Scenario - Dynamical Downscaling of CO_2-induced Climate Change in the HadCM2 GCM.

86 Rummukainen, M. (1999)
On the Climate Change debate

87 Räisänen, J. (2000)
CO_2-induced climate change in northern Europé: comparison of 12 CMIP2 experiments.

88 Engardt, M. (2000)
Sulphur simulations for East Asia using the MATCH model with meteorological data from ECMWF.

89 Persson, T. (2000)
Measurements of Solar Radiation in Sweden 1983-1998

90 Michelson, D. B., Andersson, T., Koistinen, J., Collier, C. G., Riedl, J., Szturc, J., Gjertsen, U., Nielsen, A. and Overgaard, S., (2000)
BALTEX Radar Data Centre Products and their Methodologies

91 Josefsson, W. (2000)
Measurements of total ozone 1997 – 1999

92 Andersson, T. (2000)
Boundary clear air echos in southern Sweden

93 Andersson, T. (2000)
Using the Sun to check some weather radar parameters

94 Rummukainen, M., Bergström, S., Källén, E., Moen, L., Rodhe, J. and Tjernström, M. (2000)
SWECLIM – The First Three Years

95 Meier, H. E. M. (2001)
The first Rossby Centre regional climate scenario for the Baltic Sea using a 3D coupled ice-ocean model

96 Landelius, T., Josefsson, W. and Persson, T. (2001)
A system for modelling solar radiation parameters with mesoscale spatial resolution

97 Karlsson, K.-G. (2001)
A NOAA AVHRR cloud climatology over Scandinavia covering the period 1991-2000

98 Bringfelt, B., Räisänen, J., Gollvik, S., Lindström, G., Graham, P. and Ullerstig, A., (2001)
The land surface treatment for the Rossby Centre Regional Atmospheric Climate Model - version 2 (RCA2)

99 Kauker, F. and Meier, H. E. M., (2002)
Reconstructing atmospheric surface data for the period 1902-1998 to force a coupled ocean-sea ice model of the Baltic Sea.

100 Klein, T., Bergström, R. and Persson, C. (2002)
Parameterization of dry deposition in MATCH

101 Räisänen, J., Hansson, U., Ullerstig A., Döscher, R., Graham, L. P., Jones, C., Meier, M., Samuelsson, P.and Willén, U. (2003)
GCM driven simulations of recent and future climate with the Rossby Centre coupled atmosphere - Baltic Sea regional climate model RCAO

102 Tjernström, M., Rummukainen, M., Bergström, S., Rodhe, J. och Persson, G., (2003)
Klimatmodellering och klimatscenarier ur SWECLIMs perspektiv.

103 Segersson, D. (2003)
Numerical Quantification of Driving Rain on Buildings

104 Rummukainen, M. and the SWECLIM participants (2003)
The Swedish regional climate modeling program 1996-2003. Final report.

105 Robertson, L. (2004)
Extended back-trajectories by means of adjoint equations

106 Rummukainen, M., Bergström S., Persson G., Ressner, E (2005)
Anpassningar till klimatförändringar

107 Taesler, R., Andersson, C., Nord, M (2005)
Optimizing Energy Efficiency and Indoor climate by Forecast Control of Heating Systems and Energy Management in Buildings

108 Kjellström, E., Bärring, L., Gollvik, S., Hansson, U., Jones, C., Samuelsson, P., Rummukainen, M., Ullerstig, A., Willén, U., Wyser, K., (2005)
A 140-year simulation of European climate with the new version of the Rossby Centre regional atmospheric climate model (RCA3).

109 Meier, H.E.M., Andréasson, J., Broman, B., Graham, L. P., Kjellström, E., Persson, G., and Viehhauser, M., (2006)
Climate change scenario simulations of wind, sea level, and river discharge in the Baltic Sea and Lake Mälaren region – a dynamical downscaling approach from global to local scales.

110 Wyser, K., Rummukainen, M., Strandberg, G., (2006)
Nordic regionalisation of a greenhouse-gas stabilisation scenario

111 Persson, G., Bärring, L., Kjellström, E. and Strandberg G. (2007).
Climate indices for vulnerability assessments

112 Jansson, A., Persson, Ch., Strandberg, G., (2007)
2D meso-scale re-analysis of precipitation, temperature and wind over Europe - ERAMESAN

Swedish Meteorological and Hydrological Institute
SE-601 76 Norrköping · Sweden
Tel +46 11 495 80 00 · Fax +46 11 495 80 01

ISSN 0347-2116